Formation and Catalytic Activity of Palladium Nanostructure Through the Spatially Oriented Biomineralization Peptide

（立体配向制御バイオミネラリザーションペプチドを介した

パラジウムナノ構造体の形成と触媒活性）

Laboratory of Biological Chemistry

Graduate School of Chemical Sciences and Engineering

Hokkaido University

Jose Isagani Belen Janairo

September, 2014

Table of Contents

Abbreviations

1. General Introduction

1.1. Biomineralization ……...1
1.2. Palladium……8
1.3. Electron Microscope ……..9
1.4. Circular Dichroism……..13
1.5. Aims……16
1.6. References……... 17

2. Effects of the Buffer on the Structure and Catalytic Activity of Pd Nanomaterials Formed by Biomineralization

2.1. Abstract……22
2.2. Introduction……..23
2.3. Experimental Procedures…….……25
2.4. Results…….……..27
2.4.1. Formation and characterization of the Pd nanostructures formed through biomineralization in different buffers……..27
2.4.2.Catalytic activity of the Pd nanomaterials formed from biomineralization under different buffer conditions……...32
2.5. Discussion……....35
2.6. References……....40

3. Formation of 3D Pd Nanostructure by Biomineralization Using an Oligomerized Peptide as the Control Element

3.1. Abstract……...42
3.2. Introduction…….43
3.3. Experimental Procedures…….……45
3.4. Results…….48
3.4.1. Peptide Design and Structure Analysis……...48
3.4.2. Palladium nanostructure synthesis and characterization…….……54
3.5. Discussion…….……..60
3.6. References…….……..64

4. Effects of the Biomineralization Peptide Topology on the Catalytic Activity of Pd Nanomaterials

4.1. Abstract……...…….66
4.2. Introduction……..67
4.3. Experimental Procedures…….…….68
4.4. Result…….…...69
4.4.1. Catalytic Activity of the Pd4-p53Tet Pd nanocorals…….……69
4.5. Discussion…….....75

4.6. References……...77

5. Conclusion……....……79

6. Acknowledgement……....81

Abbreviations

BF-STEM	Bright field – scanning transmission electron microscope
BMPep	Biomineralization peptide
CD	Circular dichroism
DMF	*N*,*N*,-dimethylformamide
EDX	Energy dispersive x-ray spectroscopy
Fmoc	9-fluorenylmethoxycarbonyl
GFC	Gel filtration chromatography
HBTU	2-(Benzotriazol-1-yl)-N,N,N′,N′-tetramethyluronium hexafluorophosphate
HEPES	4-(2-hydroxyethyl)-1-piperazineethanesulfonic acid
HOBt	1-hydroxybenzotriazole
HPLC	High performance liquid chromatography
HRTEM	High resolution transmission electron microscope
MALDI-TOF MS	Matrix assisted laser desorption-time of flight mass spectrometer
NMP	*N*-methyl-2-pyrrolidine
NP	Nanoparticle
p53Tet	Tetramerization domain of the tumor suppressor p53 protein
SE-STEM	Secondary electron – scanning transmission electron microscope
TFA	Trifluoroacetic acid
TOF	Turnover frequency
Tris	Tris(hydroxymethyl)aminomethane

1.0 General Introduction

1.1 Biomineralization

1.1.1 Biomineralization as a Natural Phenomenon

Inorganic structures are very important for organisms. These structures serve a variety of purposes from the simple unicellular bacteria to human beings which are essential for survival. For instance, a certain class of bacteria called magnetotactic bacteria uses iron oxide-based nanostructures as sensors to orient themselves to the external magnetic field. [1] These bacteria possess a special organelle called magnetosomes in which these specialized inorganic structures are formed. The eukaryotic unicellular diatoms mineralize silica into micro-sized shells with amazing shapes and a high degree of symmetry. [2] On a larger dimension, the bones, shells and teeth of higher forms of organisms are similarly essential inorganic structures. These structures provide mechanical support to the organism, help in nutrition-related functions and also provide defensive mechanisms. In addition to their aforementioned roles, these structures also have taxonomical significance. Mollusks possess species-specific shells that can be used as tools for their identification and proper classification. [3] This diversity in which biomineralization proceeds also manifests itself at the protein level which highlights the complexity of the process. For example, the shell matrix proteins of oysters that are highly involved in the regulation of shell and pearl formation were characterized wherein 66 out of the 80 proteins were deemed unique. [4] In spite of this seemingly complex process, a general model of biomineralization has been described by Mann. [5] The model demonstrates two possible sites of biomineralization wherein it can either occur within or outside the cell. For extracellular biomineralization, ions are encapsulated in a vesicle and shuttled out of the cell where it is deposited onto a

polymeric support. In the case for intracellular biomineralization, the ions start nucleation within the cell. Small units of the precipitated mineral are then combined with the extracellular organic matrix. In any case, both types of biomineralization share the common feature of being boundary-organized and the use of an organic matrix to direct the process. From these features the different forms of regulation are achieved such as chemical, spatial, structural, morphological and constructional control. Alienating the process within confined spaces facilitates concentration control of the different components that influences the overall property of the mineral. For instance, the shape of the spicules of the sea urchin was found to be highly dependent on the concentration of its endothelial growth factor. [6] Moreover, this feature has important implications on the manner in which the organism responds to its environment that also has an impact on biomineralization. It has been shown that silification is pH-dependent wherein the diatom *Thalassioria weissflogii* modifies its intracellular silica content in response to the pH of the environment. [7] Boundary organization also controls the size of the mineralized structure since the size of the microcompartment can dictate the overall dimensions of the biogenic mineral. On the other hand, the use of an organic matrix to induce biomineralization affects the nucleation and arrangement of the ions, [8] as in the case of collagen and bone formation. [9]

1.1.2 Biomineralization as a Synthetic Route Towards Nanomaterial Synthesis

The materials produced from nature boast of efficiency and high-performance. [10] These outstanding properties of natural materials are linked to the ability of biomineralization to precisely regulate numerous parameters during the formation process. All of these have led to the application of biomineralization for the preparation of synthetic materials. [11] Bio-inspired approaches towards the preparation of materials showcase a relatively benign and simple reaction conditions in contrast to the other known synthetic methods. [12] In addition,

it serves as an excellent alternative in the preparation of nanostructures that highlights an innovative approach integrating two disciplines together. A common method of applying biomineralization for nanostructure preparation involves the utilization of bacteria [13] and fungi. [14] Both systems exploit the ability of the microorganism to direct mineralization after which the produced materials are harvested. Another method involves the utilization of peptides and proteins as templates to guide inorganic structure growth. [15,16] The utilization of peptides was conceived out of the principal tenet of biomineralization which uses organic matrices. While different kinds and classes of organic templates have been used, [17] peptides have received special attention due to their several attractive properties. These properties include self-assembly, metal coordination and crystallographic facet recognition and binding. Peptide self-assembly can lead to a pre-organized scaffold from which structural and morphological controls during biomineralization can be attained. Peptides can recognize and bind to specific facets of the growing inorganic material which leads to shape and size control. [18] From a functional perspective, peptide templates have also been shown to have an effect on the catalytic activity of metal nanostructures. The bound peptide onto the nanostructure surface can modulate the reactivity of the nanocatalysts. [19] The diversity of biomineralization peptides makes peptide-mediated biomineralization a powerful tool for nanomaterial synthesis. Different biomineralization peptides are available for different inorganic materials (Table 1-1). In addition, different types of nanostructure can be formed by using different sequences for the same inorganic material. [20] Through this method of nanomaterial synthesis, various forms of highly active materials have been developed. Biomineralized nanostructures have been created as catalysts, [21] plasmonic materials, [22] and biomolecular recognition platforms. [23] These are just a few examples of numerous applications where biomineralized nanostructures have been highly relevant.

Table 1-1. Biomineralization peptide sequences and the type of inorganic nanostructure they form. These peptide sequences have been summarized in the review by N.L. Rosi and C.L. Chen [24].

Peptide Sequences	Inorganic Materials
NPSSLFRYLPSD	Ag nanoparticles
AHHAHHAAD	Au nanoparticles
HYPTLPLGSSTY	CoPt nanoparticles
HNKHLPSTQPLA	FePt nanoparticles
NNPMHQN	ZnS nanoparticles
SLKMPHWPHLLP	GeO_2 nanoparticles
FDFDFDFD	$CaCO_3$

Biomineralization peptides are usually discovered through peptide libraries. Phage peptide display is a powerful method in isolating peptides exhibiting binding affinity towards metal surfaces. [25] Phage peptide display has led to the identification of numerous peptide sequences that are able to support the growth of nanostructured silver, cobalt, palladium, titanium, germanium and even calcium molybdate, [26] among others. This method involves a phage library wherein peptide sequences are expressed as a fusion protein of the virus coat (Figure 1-1). The phage library is incubated with the material of choice like crystals [27] and particles. [28] After incubation, phage displaying peptides that exhibit little or no affinity towards the chosen material will be removed during the wash step. Only phage displaying peptide sequences that favor binding to the material will remain and be eluted. The collected phages will be digested and its genetic material will be amplified through PCR. This procedure is repeated several cycles and the final step involves the determination of the peptide sequence based from the DNA sequence. [29] The affinity of a target peptide towards a given inorganic surface provides the possibility that the peptide can support the growth and stabilization of nanostructures. It should be noted however that not all peptides that exhibit binding affinity to inorganic surfaces are effective templates and capping agents for nanomaterial synthesis. This is due to the possibility of ineffective elution of peptides bound to the surface during the wash step. Such was the case in a study of R. Naik and co-workers wherein only one silver-binding peptide out of three was able to support nanoparticle synthesis.[30] Moreover, the danger of false positive results is always present due to several factors such as contaminations, propagation advantage, and the like. [31]

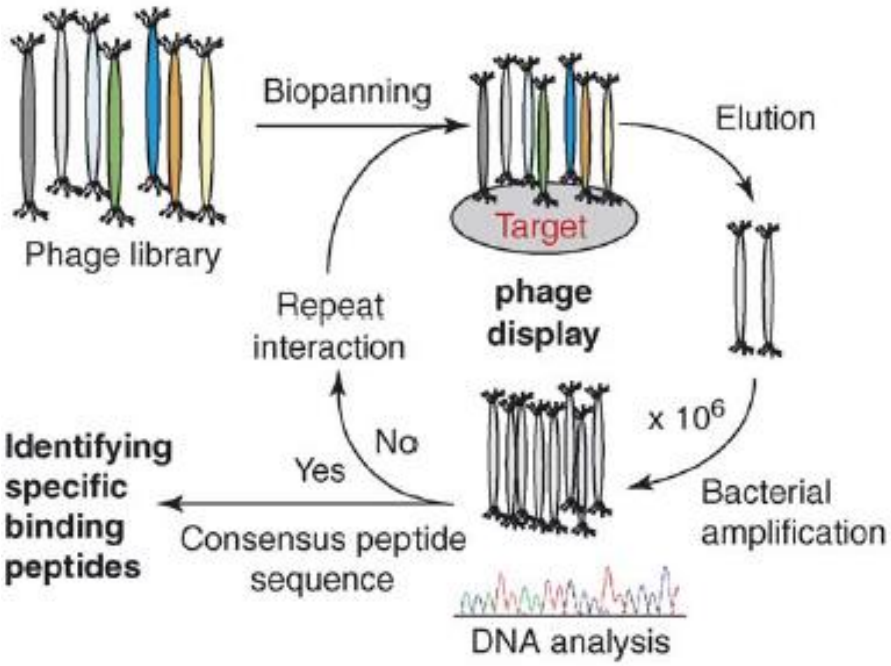

Figure 1-1. Schematic diagram of the phage-display method to identify peptide sequences that bind to the target of interest. Adapted from [32] with permission. Copyright 2006 Elsevier.

The combinatorial system of Split-and-Mix library [33] is another viable approach in discovering biomineralization peptides. Wennemers and colleagues used this method to isolate and characterize silver mineralizing peptides. [34] In their work, the Split-and-Mix system of generating a library starts by having seven equal proportions of amino acid-loaded Tentagel resins. Each proportion is encoded with an inert, unique tag or a unique combination of tag for identification and tracking of reaction history. A linker is then coupled with the on-resin amino acid followed by the addition of another set of unique tags. The third and final round involves the coupling of amino acids and tag addition. After the library has been created, the beads were then incubated with a solution of silver nitrate. Reduction with UV irradiation or ascorbic acid will lead to bead coloration if the peptide present in the bead has affinity for silver. The colored beads can then be easily picked followed by peptide identification.

Despite the success of biomineralization as a synthetic route towards nanomaterial formation, challenges and limitations are present which need to be addressed. First of which is that the interplay among several parameters during biomineralization has not been thoroughly examined. Much focus has been given on the relationship between the biomineralization peptide and the nanostructure. Although the peptide occupies the central role in biomineralization, understanding how other factors affect biomineralization is also important. Another challenge in biomineralization is how to precisely direct the three-dimensional assembly of the peptide. The 3D assembly of the peptides is the key in the proper formation of bioinspired materials since this one of the reasons behind the outstanding properties of natural materials. [11] However, methods have been scarce which can specifically assign the 3D orientation of the biomineralization peptide while simultaneously controlling other parameters. Therefore addressing these challenges will facilitate a deeper understanding of biomineralization.

1.2 Palladium

Palladium is one of the most important metals in catalysis since it is known to be involved in numerous classes of reactions. In general, Pd catalysts exhibit several attractive properties which make them key components in organic synthesis or industrial processes. The most important property of Pd is that no other transition metal can offer the same versatility in C-C bond formations. Also Pd catalysts are quite insensitive to oxygen and moisture, even to acids. [35] Pd catalysts exist as Pd(II) and Pd(0) complexes, or a combination of both valence states for reactions involving redox systems. Pd(II) complexes are square planar 16-electron complexes that are coordinatively unsaturated. This property of Pd(II) complexes render them suitable as homogeneous catalysts since they are highly labile. These complexes are able to carry out the facile coordination of reactants and loss of products from the coordination sphere. [36] Catalysis on Pd surface wherein Pd usually exists in a zero-valent state is commonly encountered in heterogeneous catalysis. Pd surfaces are known to facilitate chemisorption of reactants and on this surface is where the reaction occurs. Pd is known to be a superior catalyst for hydrogenation reactions since it is able to easily facilitate the rearrangements and transformation of the reactants. [37] Aside from functional group reductions, Pd catalysis is most known for cross coupling reactions. This type of reaction includes the Suzuki coupling, Heck reaction and Sonogashira coupling.

The usual forms of Pd catalysts used in the present time include both bulk and nanostructured Pd. Most prominent type of bulk Pd catalysts are Pd black (elemental Pd(0)), Pd/C (carbon-supported Pd) and the Lindlar catalyst (Pd in $CaCO_3$ or $BaSO_4$ treated with lead). [38] For Pd nanocatalysts, different morphologies have been reported but the most common of which is the nanoparticle. Developing highly active, selective and stable catalysts has been the focus of research involving Pd nanocatalysis. The motivation arises from the observed improved characteristics of nanostructures over bulk materials. The enhanced

catalytic activity of nanostructures in general, can be credited to the size and shape of the catalyst. The decrease in size increases the surface area of the catalyst. This basically means that for the same amount of material, nano-sized materials have more active surfaces exposed compared to larger materials. This high amount of surface atoms is the source of the reactivity of nanocatalysts. The fraction of the atoms at the surface, called dispersion has fewer neighbors compared to the atoms located internally. These surface atoms are less stable than the internal atoms and are thus more reactive in an attempt to lower their energy and achieve stability. [39] The shape of the material also has an influence on the reactivity since corner and edge atoms have higher reactivity than surface atoms. [40] The high reactivity of Pd nanocatalysts is connected with the alteration of the electronic band structure which translates into an increase in the adsorption energy of the reactants and a decrease in the dissociation barrier for the adsorbed species. [41]

1.3 The Electron Microscope (EM)

The electron microscope is the primary instrument used for the structural and morphological characterization of nanomaterials. The EM uses accelerated electrons as the illumination source whereas visible light for the conventional light microscope. This difference provides the superiority of the EM in terms of resolution since electrons have much shorter wavelengths than visible light. The relationship between wavelength and resolution in microscopy is given by the Abbe equation [42]

$$resolution = \frac{(0.612)(\lambda)}{NA}$$

Where λ is the wavelength and NA is the numerical aperture of the instrument. By using shorter wavelength, the distance between two objects that can be resolved decreases. This therefore translates into greater resolution.

1.3.1 Electron-Matter Interaction

The electrons used for illumination is produced from the electron gun and are accelerated in an electric field towards the sample. Before reaching the specimen, the electrons are focused into a beam using electromagnetic coils. The whole process is conducted in a vacuum to avoid unnecessary scattering. An electron from this beam interacts with the sample in different manners, from which different types of signals are generated. Secondary electron (SE) signals are formed inelastic collisions between the electron beam and the sample. [43] The primary electron (from the electron beam) collides with an electron in the sample which in the process transfers kinetic energy into it. This results to the ejection of the electron from the sample and this secondary electron is picked by the detector. Secondary electrons possess sensitive topographical information about the sample which makes them the method of choice for surface characterization. [44] This is because the density of secondary electrons generated is concentrated at the surface of the specimen. The primary exciting electron can also elastically collide with the specimen which forms backscattered electrons (BSE). Little energy is loss when the primary electron interacts with the nucleus of the specimen atom. This leads to scattering in all direction and hence it has no useful topographical information. However, the degree of interaction of the primary electron depends on the atomic number of the specimen. Therefore backscattered electrons carry compositional information of the sample and are useful to differentiate the elements that are contained in the specimen. Backscattered electrons that are collected by detectors are used to produce Z-contrast images or dark field images. [45] Transmitted electrons (TE) are also important sources of information for characterization. TE pass through the sample which interacts with the internal composition of the material that forms the basis of the generated image. [46] The sample however must be very thin in order for the electrons to pass through. Regions of the sample which are denser would appear darker since fewer electrons will be

able to pass through. On the other hand, thin regions will appear lighter since more electrons will be allowed to pass. This type of imaging is called bright field since the area surrounding the sample appears very bright. The first two types of electron sources are used by the Scanning Electron Microscope (SEM) whereas transmitted electrons are used by the Transmission Electron Microscope (TEM). A combination of both microscopes called Scanning Transmission Electron Microscope (STEM) is able to carry out numerous functions based on the interactions described.

Electron microscopes are commonly coupled with and an additional detector to carry out Energy Dispersive Spectroscopy (EDS). EDS is a valuable characterization method to qualitatively and quantitatively analyze the composition of the sample. EDS is also rooted in the interaction of the primary electron with the sample. The primary electron upon collision with an inner shell electron of the sample will induce it to be ejected. This process leaves a gap in the orbital. An electron from a higher energy state will then relax to fill in the gap of the ejected electron. This relaxation gives rise to the emission of characteristic x-rays. Therefore by examining the emitted x-ray, the elemental identity and amount can be determined. [47]

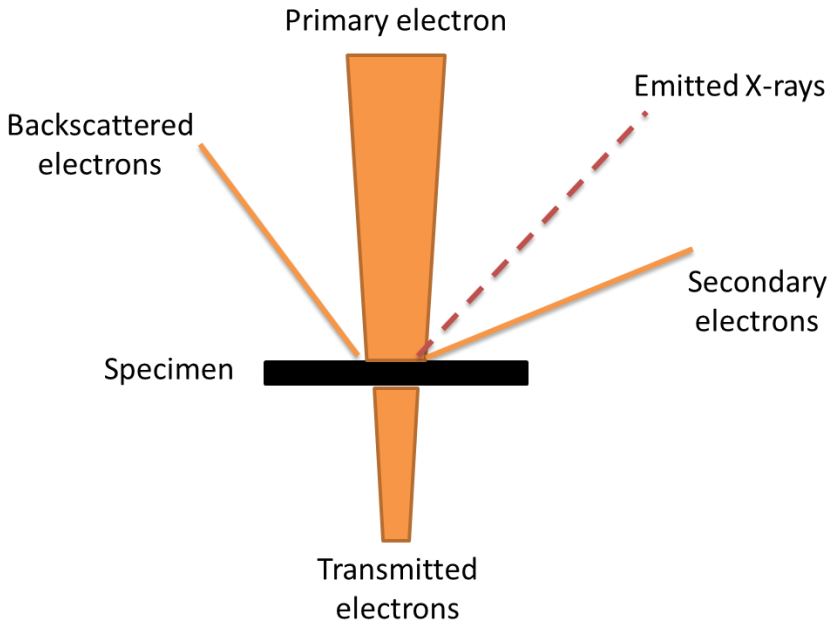

Figure 1-2. Simplified representation of the different types of signals that arise from the interaction of the electron beam with the specimen.

1.4 Circular Dichroism (CD) Spectroscopy

CD spectroscopy is an effective method to probe and determine the secondary structures and conformations of biomolecules like peptides and proteins. This method exploits the absorption disparity of chiral molecules towards circularly polarized light. [48] CD spectrometers produce left circularly polarized light and right circularly polarized light. A chiral molecule exhibits absorption preference towards circularly polarized light. The difference between the absorption of both types of circularly polarized light is called circular dichroism. Data from CD spectroscopic measurements can be broadly classified into two types, namely circular dichroism and ellipticity. [49] As mentioned above, CD is the difference in absorption between left and right circularly polarized light; and can be defined as:

$$\Delta A = A(LCP) - A(RCP)$$

By invoking Beer's law, molar CD (Δε) is expressed as:

$$\Delta\varepsilon = \varepsilon(LCP) - \varepsilon(RCP)$$

$$\Delta\varepsilon = \frac{\Delta A}{bC}$$

Where b is the cell path length and C is the analyte concentration. A variation of this unit which is specifically used for proteins is the mean residue molar circular dichroism (ΔεMR). Here, circular dichroism is reported in terms of the amount of amino acid residues of the protein instead of the absolute protein concentration. This is convenient in comparing different proteins each possessing varying numbers of residues. It is calculated by:

$$mean\ residue\ concentration\ (MRC) = \frac{protein\ concentration}{number\ of\ residues}$$

$$\Delta\varepsilon MR = \frac{\Delta A}{(MRC)(b)}$$

Circular dichroism can also be expressed in terms of ellipticity (θ). Since CD arises from an absorption preference for a type of circularly polarized light, elliptically polarized light results. This is because the left and right circularly polarized light that passed through the sample now has different amplitudes. The relationship between ΔA and θ is expressed as

$$\Delta A = \frac{\theta}{32.982}$$

Although large biomolecules are made up of chiral molecules, relevant signals are obtained due to the interaction of polarized light with the entire three-dimensional structure of the biomolecule. Each type of secondary structure has a unique CD signal within the UV and visible regions. These signatures are utilized in various ways such as identification of a structural motif, monitoring the change in a particular structural motif as a function of other parameters, and so on (Figure 1-3). [50]

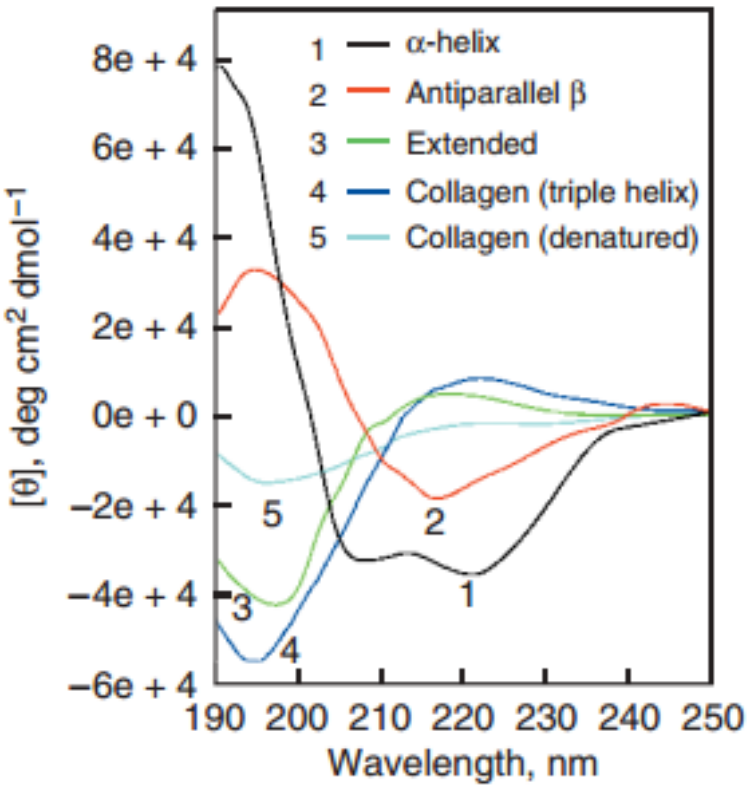

Figure 1-3. Representative CD spectra of peptides showing the typical spectral profile for the different secondary structures. Adapted from [50] with permission. Copyright 2006 Nature Publishing Group

1.5 Aims

The presented study aims to evaluate the effect of precisely defining the spatial orientation, arrangement and valency of the biomineralization peptide on the produced nanostructures. Given the importance of palladium in numerous applications especially in catalysis, biomineralization of palladium was chosen as the system to test the hypothesis that defining the abovementioned parameters will have an effect on the structure and catalytic activity of the biomineralization products. Similarly, the effect of buffer on the structure and catalytic activity of the biomineralization products was also analyzed. The parameters examined in this study, namely the topological property of the biomineralization peptide and the type of buffer are very important factors related to biomineralization. Arrangement and orientation are important features of natural materials. On the other hand, maintaining the pH of the system through buffers is important every time peptides are involved. Therefore, this study is expected to contribute to the deeper understanding of biomineralization as a method to synthesize materials.

1.6 References

1. L.Yan, S. Zhang, P. Chen, H. Liu, H. Yin, H. Li. Magnetotactic bacteria, magnetosomes and their application. *Microbiol. Res.* **2012**, 167, 507-519.
2. M. Hildebrand, Diatoms, biomineralization, processes and genomics. *Chem. Rev.* **2008**, 108, 4855-4874.
3. I.M. Weiss, Species-specific shells: Chitin synthases and cell mechanics in molluscs. *Z. Kristallogr.* **2012**, 227, 723-728.
4. B. Marie, C. Joubert, A. Tayale, I. Zanella-Cleon, C. Belliard, D. Piquemal, N. Cochennec-Laureau, Y. Gueguen, C. Montagnani. Different secretory repertoires control biomineralization processes of prism and nacre deposition of the pearl oyster shell. *Proc. Natl. Acad. Sci. U.S.A.* **2012**, 109, 20986-20991.
5. S. Mann, *Biomineralization: Principles and Concepts in Bioinorganic Materials Chemistry,* Oxford Univ. Press: UK, 2001.
6. R.T. Knapp, C.H. Wu, K.C. Mobilia, D. Joester. Recombinant sea urchin vascular endothelial growth factor directs single-crystal growth and branching in vivo. *J. Am. Chem. Soc.* **2012**, 134, 17908-17911.
7. V. Herve, J. Derr, S. Douady, M. Quinet, L. Moisan, P.J. Lopez. Multiparametric analyses reveal the pH-dependence of silicon biomineralization in diatoms. *PLos One*. **2012**, 7, e46722.
8. S. Mann. Molecular recognition in biomineralization. *Nature*. **1988**, 332, 119-124.
9. Y. Wang, T. Azais, M. Robin, A. Vallee, C. Catania, P. Legriel, G. Pehau-Arnaudet, F. Babonneau, M.M. Giraud-Guille,N. Nassif. The predominant role of collagen in the nucleation, growth, structure and orientation of bone apatite. *Nat. Mater.* **2012**, 11, 724-733.

10. B. Bhusan. Biomimetics: lessons from nature- an overview. *Phil. Trans. R. Soc. A.* **2009**, 367, 1445-1486.
11. F. Nudelman, N.A.J.M. Sommerdijk. Biomineralization as an inspiration for materials chemistry. *Angew. Chem. Int. Ed.* **2012**, 51, 6582-6596.
12. S.G. Kwon, T. Hyeon. Colloidal chemical synthesis and formation kinetics of uniformly sized nanocrystals of metals, oxides and chalcogenides. *Acc. Chem. Res.* **2008**, 41, 1696-1709.
13. C.S. Butler, C.M. Debieux, E.J. Dridge, P. Splatt, M. Wright. Biomineralization of selenium by the selenite-respiring bacterium Thauera selenatis. *Biochem. Soc. Trans.* **2012**, 40, 1239-1243.
14. S. Das, J. Liang, M. Schmidt, F. Laffir, E. Marsili. Biomineralization mechanism of gold by zygomycete fungi Rhyziporous oryzae. *ACS Nano*. **2012**, 6, 6165-6173.
15. A. Schulz, H. Wang, P. van Rijn, A. Boker. Synthetic inorganic materials by mimicking biomineralization processes using native and non-native protein functions. *J. Mater. Chem.* **2011**, 21, 18903 – 18918.
16. B. Briggs, M.R. Knecht. Nanotechnology meets biology: peptide-based methods for the fabrication of functional materials. *J. Phys. Chem. Lett.* **2012**, 3, 405-418.
17. K. van Bommel, A. Friggeri, S. Shinkai. Organic templates for the generation of inorganic materials. *Angew. Chem. Int. Ed.* **2003**, 42, 980-999.
18. C.Y. Chiu, Y. Li, L. Ruan, X. Ye, C.B. Murray, Y. Huang. Platinum nanocrystals selectively shaped using facet-specific peptide sequences. *Nat. Chem.* **2011**, 3, 393-399.
19. Y. Li, Z. Tang, P.N. Prasad, M.R. Knecht, M.T. Swihart. Peptide-mediated synthesis of gold nanoparticles: effects of peptide sequence and nature of binding on physicochemical properties. *Nanoscale*. **2014**, 6, 3165-3172.

20. N. Choi, L. Tan, J. Jang, Y.M. Um, P.J. Yoo, W-S. Choe. The interplay of peptide sequence and local structure in TiO2 biomineralization. *J. Inorg. Biochem.* **2012**, 115, 20-27.

21. D.B. Pacardo, M. Sethi, S.E. Jones, R.R. Naik, M.R. Knecht. Biomimetic synthesis of Pd nanocatalysts for the Stille coupling reaction. *ACS Nano*. **2009**, 3, 1288-1296.

22. C. Song, M.G. Blaber, G. Zhao, P. Zhang, H.C. Fry, G.C. Schatz, N.L. Rosi. Tailorable plasmonic circular dichroism properties of helical nanoparticle superstructures. *Nano Lett.* **2013**, 13, 3256-3261.

23. J.M Slocik, M.O. Stone, R.R. Naik. Synthesis of gold nanoparticles using multifunctional peptides. *Small*. **2005**, 1,1048-1052.

24. C.L. Chen, N.L. Rosi. Peptide-based methods for the preparation of nanostructured inorganic materials. *Angew. Chem. Int. Ed.* **2010**, 49, 1924-1942.

25. T. Douglas, M. Young. Viruses: making friends with olds foes. *Science*. **2006**, 312, 873-875.

26. G. Ahmad, M. B. Dickerson, B. C. Church, Y. Cai, S. E. Jones, R. R. Naik, J.S. King, C.J. Summers, N. Kroger, K.H. Sandhage. Rapid-room temperature formation of crystalline calcium molybdate phosphor microparticles via peptide-induced precipitation. *Adv. Mater.* **2006**, 18, 1759-1763.

27. S.R. Whaley, D.S. English, E.L. Hu, P.F. Barabara, A.M. Belcher. Selection of peptides with semiconductor binding specificity for directed nanocrystal assembly. *Nature*. **2000**, 405, 665-668.

28. K. Sano, K. Shiba. A hexapeptide motif that electrostatically binds to the surface of titanium. *J. Am. Chem. Soc.* **2003**. 125, 14234-14235.

29. R.R. Naik, S.E. Jones, C.J. Murray, J.C. McAuliffe, R.A. Vaia, M.O. Stone. Peptide templates for nanoparticle synthesis derived from polymerase chain reaction-driven phage display. *Adv. Funct. Mater.* **2004** 14, 25-30.

30. R.R., Naik, S.J. Stringer, G. Agarawal, S.E. Jones, M.O. Stone. Biomimetic synthesis and patterning of silver nanoparticles. *Nature Mater.* **2002**. 1, 169-172.

31. M. Vodnik, U. Zager, B. Strukelj, M. Lunder, M. Phage display: selecting straws instead of a needle from a haystack. *Molecules*. **2011**. 16, 790-817.

32. A. Merzlyak, S.W. Lee. Phage templates for hybrid materials and mediators for nanomaterial synthesis. *Curr. Opin. Chem. Biol.* **2006**, 10, 246-252.

33. K.S. Lam, S.E. Salmon, E.M. Hersh, V.J. Hruby, W.M. Kazmierski, R.J. Knapp. A new type of synthetic peptide library for identifying ligand-binding activity. *Nature.* **1991**. 354, 82-84.

34. K. Belser, T.V. Slenters, C. Pfumbidzai, G. Upert, L. Mirolo, K.M. Fromm, H. Wennemers. Silver nanoparticle formation in different sizes induced by peptides identified within split-and-mix libraries. *Angew. Chem. Int. Ed.* **2009**. 48, 3661-3664.

35. J. Tsuji, *Palladium Reagents and Catalysts*, John Wiley & Sons: UK, 2004.

36. D.F. Shriver and P.W. Atkins, *Inorganic Chemistry, 3rd Edition*, Oxford University Press: UK, 1999.

37. G. Brieger, T. J. Nestrick. Catalytic transfer hydrogenation. *Chem. Rev.* **1974**. 5, 567-580.

38. H. Lindlar. Ein neuer Katalysator für selektive Hydrierungen. *Helv. Chim. Acta.* **1952**. 35, 446.

39. E.Roudner. Size matters: why nanomaterials are different. *Chem. Soc. Rev.* **2006**. 35, 583-592.

40. A. Fihri, M. Boughrara, B. Nekoueishahraki, J.M. Basset, V. Polshettiwar. Nanocatalysts for Suzuki cross-coupling reactions. *Chem. Soc. Rev.* **2011**. 40, 5181-5203.

41. C.R. Henry, in *Nanocatalysis*, ed. by U. Heiz, U. Landman, Springer, Berlin, **2007**, p. 245
42. E. Abbe. Beiträge zur Theorie des Mikroskops und der mikroskopischen Wahrnehmung. *Archiv für Mikroskopische Anatomie.* **1873**, 9, 413-4180.
43. K. Sujata, H.M. Jennings. Advances in electron microscopy. *MRS Bulletin*. **1991**, 16, 41-45.
44. A. Bogner, P-H. Jouneau, G. Thollet, D. Basset, C. Gauthier. A history of scanning electron microscopy developments: towards "wet-STEM" imaging. *Micron*. **2007**, 38, 390-401.
45. S.J. Pennycook. Z-contrast STEM for material science. *Ultramicroscopy*. **1989**, 30, 58-69.
46. R. Mammadov, A.B. Tekinay, A. Dana, M.O. Guler. Microscopic characterization of peptide nanostructures. *Micron*. **2012**, 43, 69-84.
47. C.N.R. Rao, K. Biswas. Characterization of nanomaterials by physical methods. *Annu. Rev. Anal. Chem.* **2009**, 2, 435-462.
48. S.M. Kelly, N.C. Price. The use of circular dichroism in the investigation of protein structure and function. *Curr. Protein Pept. Sci.* **2000**, 1, 349-384.
49. S.M. Kelly, T.J. Jess, N.C. Price. How to study proteins by circular dichroism. *Biochim Biophys Acta*. **2005**, 1751, 119-139.
50. N.J. Greenfield. Using circular dichroism spectra to estimate protein secondary structure *Nat. Protoc.* **2006**, 1, 2876- 2890.

2.0 Effects of the Buffer on the Structure and Catalytic Activity of Pd Nanomaterials Formed by Biomineralization

2.1 Abstract

The effect of the buffer on the structure and catalytic activity of Pd nanostructures obtained from biomineralization was evaluated. Significant structural differences attributed to the buffer were observed. The Pd nanomaterials produced from unbuffered biomineralization were severely aggregated in contrast to those formed in the presence of either Tris or HEPES. Tris-buffered biomineralization produced dispersed particles whereas HEPES-buffered biomineralization afforded large and linked particles. In addition, the Pd nanostructures prepared in buffered solutions had enhanced catalytic activity in the reduction of nitroaminophenol isomers. The enhancement in the catalytic activity can be possibly attributed to the non-aggregated nature of the Pd nanomaterials formed from buffered biomineralization. Our findings emphasize that the buffer selection is critical for biomineralization. Moreover, these indicate that the buffer can be possibly used to control the structure and activity of Pd nanomaterials which is a very simple and cost-effective way compared with other methods.

2.2 Introduction

Metal nanostructures have found increased interest in a wide variety of applications especially in catalysis due to the improved performance over their bulk counterparts. [1] Palladium nanostructures are highly sought after since Pd is known to catalyze diverse class of reactions ranging from C-C bond formation to functional group reduction. [2] Various methods are available to synthesize metallic nanostructures that include the use of polymer templates, stabilizers and surfactants. [3] Among these methods, biomineralization is an emerging technique of inorganic nanomaterial synthesis that relies on biomineralization peptides (BMPep) for the regulation of the nanostructure. [4] Biomineralization has been applied to form nanostructures of different metals such as Pd, Ag, Au, Ti, Pt, among others by using various metal-specific BMPep. [5] However, the interplay among several factors involved in biomineralization still remains largely unknown. Although it has been established that the sequence of the BMPep affects the structure and catalytic activity of the resulting nanomaterial, [6] the effect of other synthetic parameters on the biomineralized product has not been thoroughly examined. Buffers are very important components of biomineralization due to the sensitivity of the overall properties of the BMPep with the pH. Since several buffers with different properties are available at identical pH ranges, we determined the effect of buffer on the resulting palladium nanostructure produced through biomineralization. In this study, a 12-resiude BMPep (TSNAVHPTLRHL-amide) was used to direct the formation of Pd nanostructures. This BMPep, termed as Pd4, was discovered through a phage display assay. [7] This sequence is well-studied and frequently utilized for Pd biomineralization. However, previous studies that used this BMPep conducted biomineralization only in water. [6-9] In addition, we also examined the effect of these buffer-related structural changes on the catalytic activity of the Pd nanostructures. Analyzing how this parameter affects the

properties of the biomineralized products is very important since biomineralization will be better understood which can potentially lead to the formation of improved materials.

2.3 Experimental Procedure

2.3.1 Chemicals. All Fmoc-protected amino acids and the rink amide resin used were obtained from Novabiochem whereas the other reagents used in the peptide synthesis such as HOBt, HBTU, piperidine, TFA and solvents were purchased from Watanabe Chem. Ind. Ltd. $NaBH_4$ and Tris buffer were purchased from Nacalai-Tesque, K_2PdCl_4 and HEPES were both obtained from Sigma-Aldrich. All purchased reagents were used as received without further purification. Milli-Q water was used throughout all experiments.

2.3.2 Peptide Synthesis and Characterization. The Pd4 BMPep (TSNAVHPTLRHL-amide) was synthesized using an Applied Biosystems 433A automated peptide synthesizer utilizing the standard Fmoc synthetic strategy on a rink amide resin. The cleaved peptide obtained after treatment with Reagent K (9 mL trifluroacetic acid (TFA), 0.5 mL milli-Q, 0.5 mL phenol, 0.5 mL thioanisole and 0.25 mL of ethanedithiol) was purified using a Shimadzu LC-6AD HPLC equipped with a 22 x 250 mm^2 Vydac C8 column with a binary gradient of buffered MeCN/H_2O as the solvent system. The purified peptides were characterized using an Applied Biosystems Voyager 4379 MALDI-TOF MS.

2.3.3 Biomineralization reaction. Biomineralization was conducted with a 40 µM BMPep in Milli-Q water or 2.5 mM buffered solution at pH 7.4. Two buffers were used in this study, 4-(2-hydroxyethyl)-1-piperazineethanesulfonic acid (HEPES) and tris(hydroxymethyl)aminomethane (Tris). A five-fold equivalence of K_2PdCl_4 was then added into the BMPep solution and after 45 minutes, a four-fold excess of $NaBH_4$ was added. After 90 minutes, the pH of the crude biomineralization solution was measured using a pH paper. Reduction was quenched after 90 minutes through the 10-fold dilution of the solution with water to destroy the excess reductant.

2.3.4 Electron microscopy. Structural characterization was performed using a scanning transmission electron microscope (Hitachi HD-2000) operating at an acceleration voltage of 200 kV. Samples for characterization were purified by centrifugation. The purified, re-suspended materials were then placed on a carbon-coated copper grid.

2.3.5 UV-vis measurements. UV-vis spectra of the crude, diluted biomineralization products were obtained using a Jasco V-630 spectrophotometer in a glass cuvette after background subtraction.

2.3.6 Catalytic Reaction. The catalytic activity of the materials was determined using the reduction of nitroaminophenol as the model reaction. The substrates used were the isomers 2-amino-4-nitrophenol (λ_{max} = 443 nm) and 4-amino-2-nitrophenol (λ_{max} = 481 nm) in which $NaBH_4$ serves as the reducing agent. In the absence of a metal catalyst, the reduction of the substrates to 2,4-diaminophenol does not occur. The reaction is monitored by time-resolved UV-vis measurements. In a typical experiment, 10 µL of a 5 mM substrate dissolved in ethanol was added in an aqueous solution containing 10 mM of $NaBH_4$. Upon the addition of the Pd nanomaterials corresponding to 1 mol % Pd, UV-vis measurements were immediately recorded in a glass cuvette.

2.4 Results

2.4.1 Formation and characterization of the Pd nanostructures formed through biomineralization in different buffers

Structural differences that can be attributed to the influence of the presence of a buffer were clearly observed for the Pd4 biomineralization products. In the absence of any buffer, disordered, aggregated particles were formed using the Pd4 BMPep (Fig. 2-1 A & B). The average particle size was 27.2 ± 10 nm with a broad size distribution (Fig. 2-3A).The surface of the materials was uneven and irregular (Fig. 2-2 A & B). On the other hand, conducting biomineralization in a Tris-buffered medium yielded fused particles (Fig. 2-1 C & D). The particle size distribution was narrow wherein the size was found to be 30.5 ± 4 nm (Fig. 2-3B). The appearance of the particles is very different from the structures obtained under unbuffered conditions. The particle surface depicts a smooth spherical characteristic (Fig. 2-2 C & D). For the HEPES-buffered biomineralization, large, spherical and fused particles were formed (Fig. 2-1 E & F). The fused particles resembled solid chains which were 75.3 ± 9 nm in size (Fig. 2-3C). The size distribution is not as narrow relative to the particles from Tris-buffered biomineralization. The surface of the materials is smooth and even (Fig. 2-2 E & F). These particles are very different from the structures obtained under the previous two conditions with respect to size and shape. The UV-vis spectra of the Pd nanostructures from buffered and unbuffered biomineralization (Fig. 2-4) exhibited the typical spectra for nano-sized Pd, as expected. The continuous absorption along the visible and near-UV regions coincides with the calculated spectrum of Pd nanostructures using the Mie theory. [10]

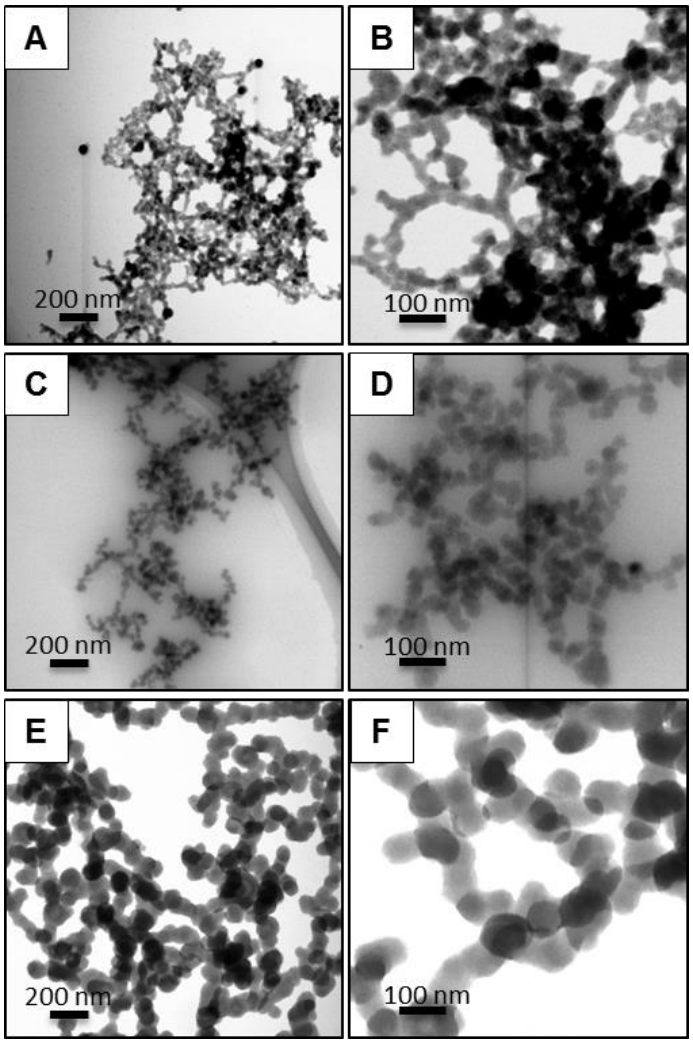

Figure 2-1. BF-STEM images of Pd nanostructures produced using the Pd4 BMPep. **A,B)** No Buffer; **C,D)** Tris; **E,F)** HEPES

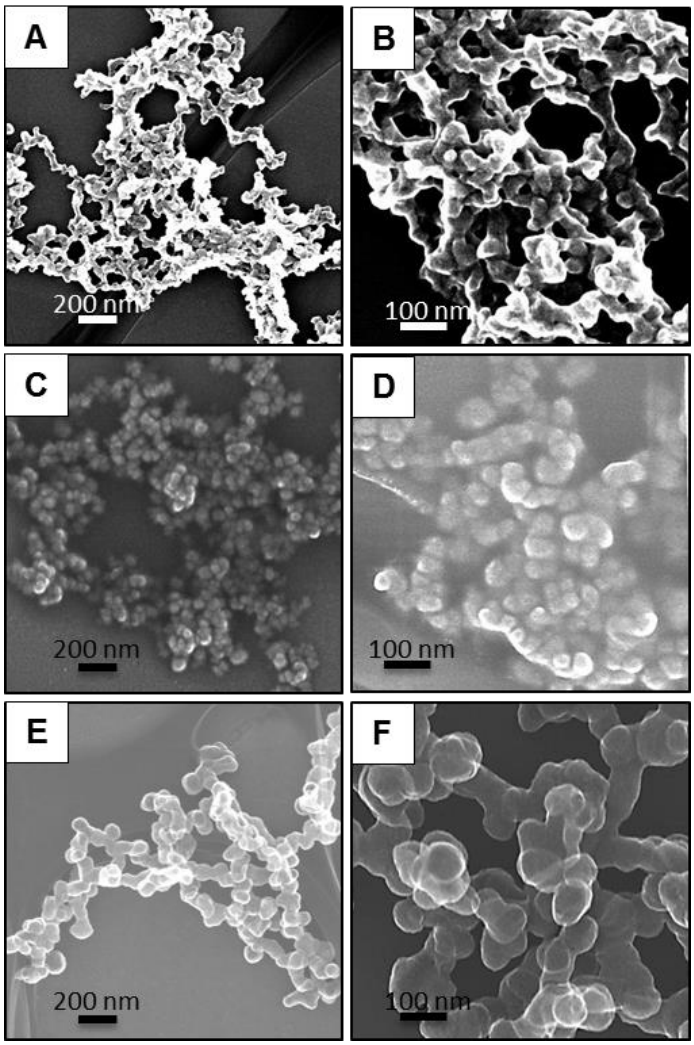

Figure 2-2. SE-STEM images of Pd nanostructures produced using the Pd4 BMPep. **A,B)** No Buffer; **C,D)** Tris; **E,F)** HEPES

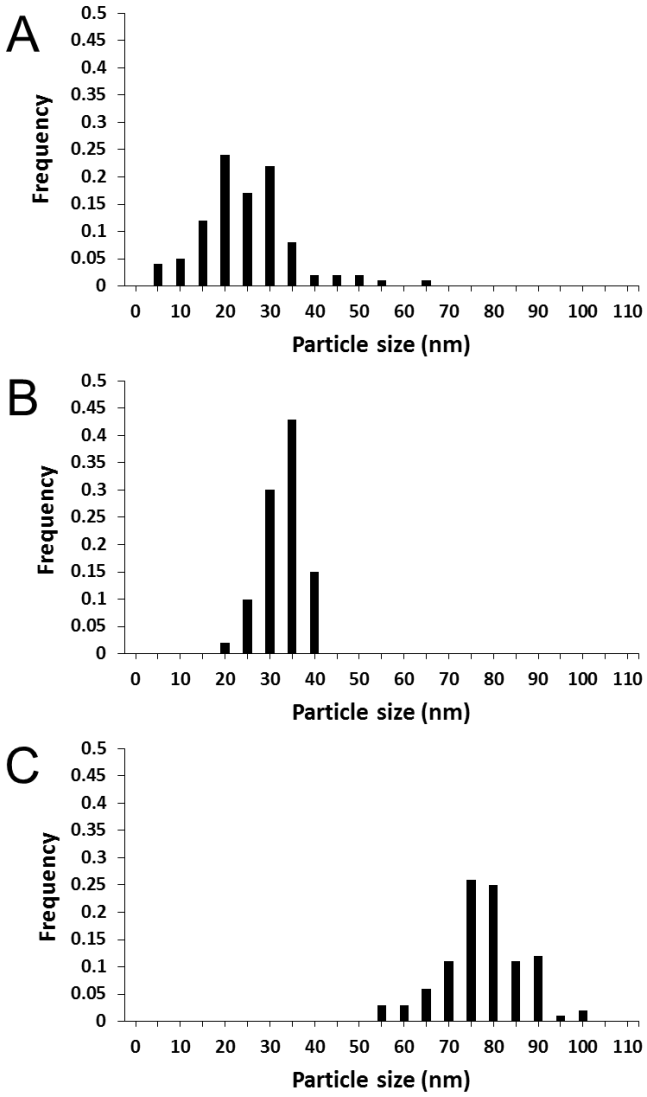

Figure 2-3. Size distribution histogram of 100 particles. Histogram increment is 5 nm. **A)** No buffer, **B)** Tris, **C)** HEPES

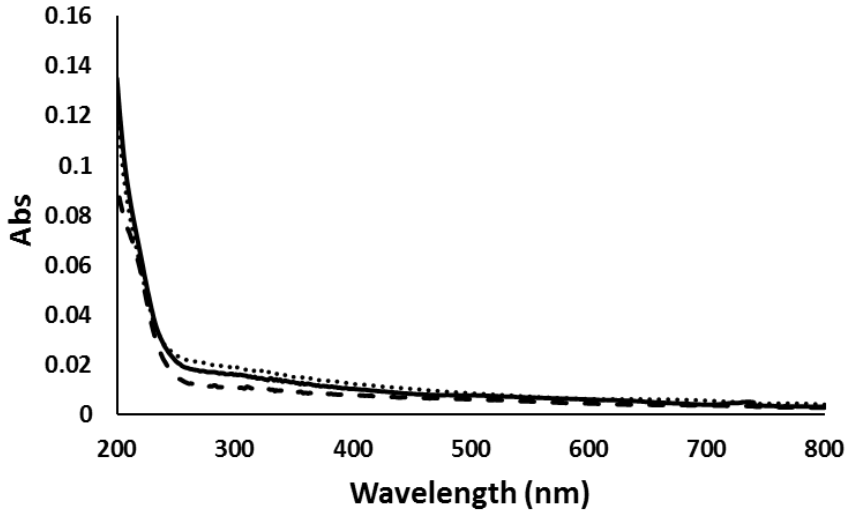

Figure 2-4. UV-vis spectra of the Pd nanostructures obtained from biomineralization using the Pd4 BMPep. Solid line = No Buffer; dotted line = Tris; dashed line = HEPES

2.4.2 Catalytic activity of the Pd nanomaterials formed from biomineralization under different buffer conditions.

Since the nanostructures obtained in the presence of buffer had varying shapes and sizes, it can be thus expected that differences in activity will be observed. The catalytic activity of the materials was determined using the reduction of nitroaminophenol as the model reaction (Scheme 2-1). The Pd nanomaterials prepared under the buffered conditions exhibited higher turnover frequency (TOF) compared to the materials prepared under the unbuffered condition (Fig. 2-5).

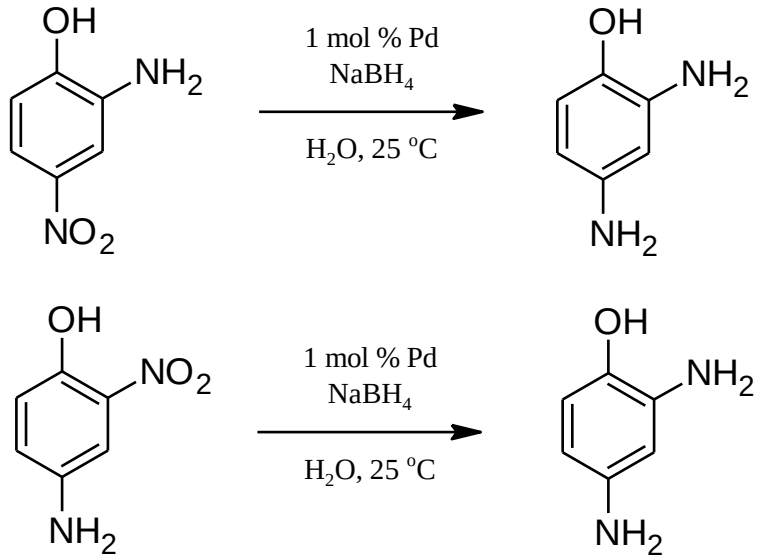

Scheme 2-1. Reduction of the nitroaminophenol substrates used for the catalytic activity determination.

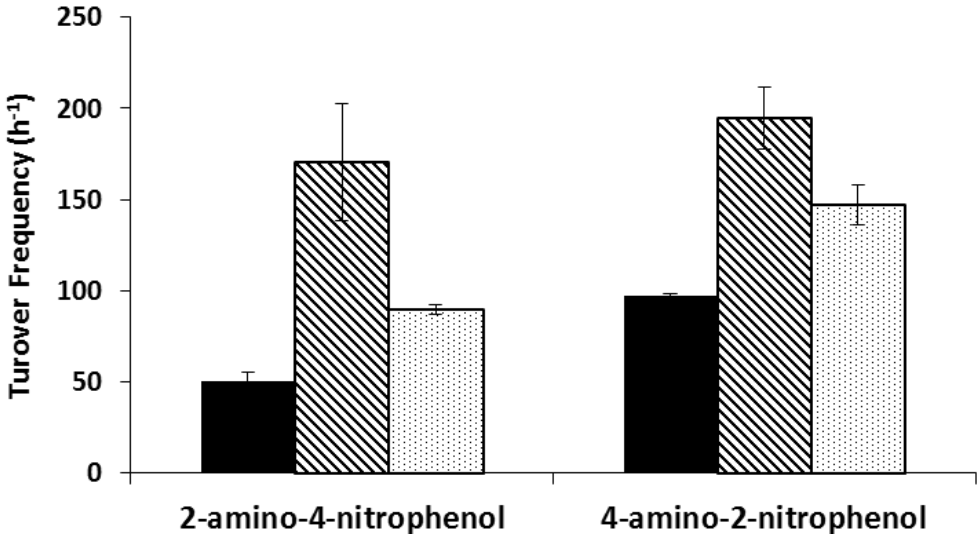

Figure 2-5. Turnover frequency of the Pd nanostructures formed from biomineralization using the Pd4 BMPep. Reaction is the reduction of nitroaminophenol isomers. [Substrate] = 50 μM, [Pd] = 1 mol %, [$NaBH_4$] = 10 mM, 25^0C, triplicate analyses. Solid fill= No Buffer; diagonal striped pattern= Tris; dotted pattern = HEPES

2.5 Discussion

The observed different Pd nanostructure indicate that the presence of the buffers influenced peptide-mediated Pd biomineralization. HEPES and Tris were used since these are very common buffers which are often used in biological experiments. Their respective buffering range overlaps and their chemical structures are different from one another. In addition, pH 7.4 was chosen since the phage display screening for the Pd4 BMPep was conducted at around neutral pH. [9] It is reported that the Pd4 BMPep produce Pd nanostructures through a capping mechanism. [8] The interaction of peptides with metals is pH dependent. This is due to the dependence of the protonation states of the side chains which can also affect peptide conformations. [11] Hence, a fluctuating environment pH can lead to a non-uniform binding of the BMPep onto the growing nanostructure surface. Under the unbuffered condition, the pH of the solution dropped to approximately 4 upon the dissolution of the BMPep. After biomineralization, the pH changed to 3. This explains the random and aggregated appearance of the nanostructures produced from unbuffered biomineralization, in addition to the very broad size distribution. Under buffered conditions, the pH of the system is maintained all throughout biomineralization or changes are minimized. The pH of the biomineralization solution after 90 minutes of reduction was maintained at around 7 in both of the buffered media. This leads to a more uniform adsorption behavior of the BMPep towards the growing material. The buffer can also participate in the stabilization of the nanoparticle. This is possible through the three hydroxyl moieties and a primary amine of Tris which can bind to the surface of Pd (Fig. 2-6A). [12] In addition to a hydroxyl group, HEPES also has a sulfonic acid moiety which can bind with metal surfaces like Pd (Fig. 2-6B). [13-15] The variation in the nanostructure produced under different buffer conditions possibly emanates from the difference in the pH of the system as well as in the structure, number and type of binding groups of the buffer. In addition, the

bound buffer on the particle surface can influence the binding behavior of the BMPep on the growing particle. [16] It can be thus expected that the Pd4 binding is different between the two types of buffers used. Taken together, the results indicate that maintaining the pH during biomineralization is critical. In addition, the data suggests that using different types of buffer can yield biomineralization products with varying structures. Therefore buffer selection is also very important for biomineralization.

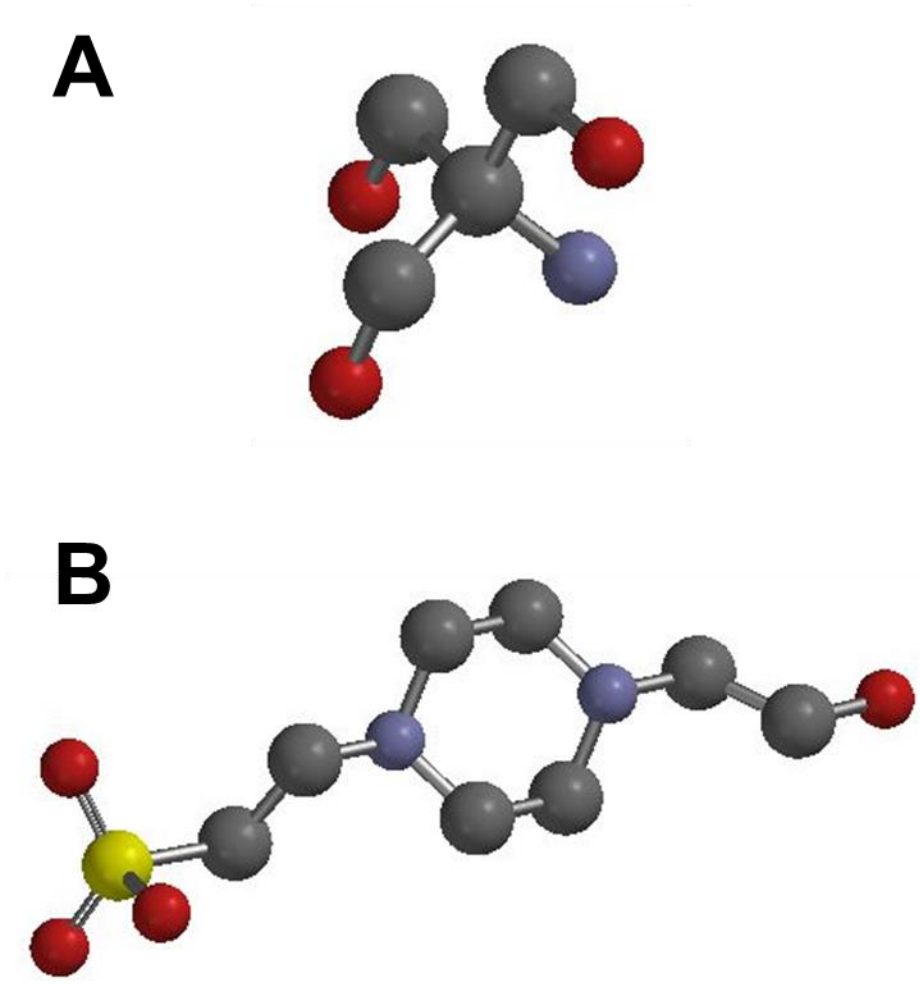

Figure 2-6. Chemical structures of **A)** Tris and **B)** HEPES buffers. Gray = carbon, red = oxygen, purple = nitrogen, yellow = sulfur. Hydrogen atoms were explicitly removed for clarity.

The materials prepared from unbuffered biomineralization were the least active since the structure is mainly aggregated. Aggregation leads to catalyst deactivation since less amount of active surface is exposed and available for reaction. [17] The high reactivity of the nanoparticles from Tris-buffered biomineralization for both substrates can be accounted for their size. Smaller particles have higher surface area compared with larger particles. The surface, corner and edge areas of the nanoparticles are the reactive sites. [18] Therefore if a particle has a higher surface area, more of these sites are exposed which translates into higher activity. Such is the reason why the nanoparticles from HEPES-buffered biomineralization are more active than the aggregated materials from unbuffered biomineralization but less active than the materials derived under Tris conditions. All of the nanomaterials exhibited slight preference towards 4-amino-2-nitrophenol on the basis of higher TOF for this substrate. It is reasonable to assume that the binding of 4-amino-2-nitrophenol onto the catalyst surface is more favored over 2-amino-4-nitrophenol. Such an assumption is plausible since the reduction of nitroarenes follows an adsorption-reaction-desorption mechanism. [19] The nitro moiety must be adsorbed onto the catalyst surface after which the reaction takes place. Upon reduction, the product desorbs from the surface. The collective catalytic data indicate that the buffer-related structural differences of the biomineralization products are significant enou gh to affect their catalytic activity as well. Our results demonstrate that the buffer type can be used as a tunable parameter in order to modulate the structure and catalytic activity of the nanomaterials produced through biomineralization. This step is very simple and easy to carry out. For Pd4 BMPep-mediated biomineralization, catalytic enhancement was observed when amino acid residue substitutions were done. [6,9] Performing biomineralization in buffered solutions is far easier and more cost-effective than synthesizing different Pd4 BMPep analogs. Further studies are still however required to fully elucidate the precise mechanism behind the

effect of the buffer on palladium biomineralization, as well as how the differences on nanostructure and the buffer type influence the catalytic properties.

2.6 References

1. Fihri, M. Bouhrara, B. Nekoueishahraki, J.M. Basset, V. Polshettiwar. Nanocatalysts for Suzuki cross-coupling reactions. *Chem. Soc. Rev.* **2011**, 40, 5181-5203.
2. *Palladium Reagents and Catalysts*, by J. Tsuji, Wiley, England, **2004**.
3. Balanta, C. Goddard, C. Claver. Pd nanoparticles for C-C coupling reactions. *Chem. Soc. Rev.* **2011**, 40, 4973-4985.
4. F. Nudelman, N. A. J. M. Sommerdijk. Biomineralization as an inspiration for materials chemistry. *Angew. Chem. Int. Ed.* 2012, **51**, 6582-6596.
5. C.L. Chen, N.L Rosi, N. Peptide-based methods for the preparation of nanostructured inorganic materials. *Angew. Chem. Int. Ed.* **2010**, 49, 2-21.
6. R. Coppage, J.M. Slocik, B.D. Briggs, A. I. Frenkel, R. R. Naik, M.R. Knecht. Determining peptide sequence effects that control the size, structure and function of nanoparticles. *ACS Nano*. **2012**, *6*, 1625-1636.
7. D.B. Pacardo, M. Sethi, S.E. Jones, R.R. Naik, M.R. Knecht. Biomimetic synthesis of Pd nanocatalysts for the Stille coupling reaction. *ACS Nano*. **2009**, 3, 1288-1296.
8. R. Coppage, J.M. Slocik, B.D. Briggs, A.I. Frenkel, H. Heinz, R.R. Naik, M.R. Knecht. Crystallographic recognition controls peptide binding for bio-based nanomaterials. *J. Am. Chem. Soc.* **2011**, *133*, 12346-12349.
9. R. Coppage, J. M. Slocik, M. Sethi, D.B. Pacardo, R.R Naik, M.R. Knecht. Elucidation of peptide effects that control the activity of nanoparticles. *Angew. Chem. Int. Ed.* **2010,** 49, 3767-3769.
10. J.A. Creighton, D.G. Eadon. Ultraviolet-visible absorption spectra of the colloidal metallic elements. *J. Chem. Soc. Faraday Trans.* **1991**, 87, 3881-3891.
11. Vallee, V. Humboldt, C.M. Pradier. Peptide interactions with metal and oxide surfaces. *Acc. Chem. Res.* **2010**, 43, 1297.

12. C.Y. Chiu, Y. Li, Y. Huang. Size-controlled synthesis of Pd nanocrystals using a specific multifunctional peptide. *Nanoscale*. **2010**, 2, 927-930.
13. C. Yee, G. Kataby, A. Ulman, T. Prozorov, H. White, A. King, M. Rafailovich, J. Sokolov, A. Gedanken. Self-assembled monolayers of alkanesulfonic acid and phosphonic acids on amorphous iron oxide nanoparticles. *Langmuir*. **1999**, 15, 7111-7115.
14. T.T. Isimjan, Q. He, Y. Liu, J. Zhu, R.J. Puddephatt, D.J. Anderson. Nanocomposite catalyst with palladium nanoparticles encapsulated in a polymeric acid: a model for tandem environmental catalysis. *ACS Sustainable Chem. Eng.* **2013**, 1, 381.
15. H. Naohara, Y. Okamoto, N. Toshima. Preparation and electrocatalytic activity of palladium-platinum core-shell nanoalloys protected by perfluorinated sulfonic acid ionomer. *J. Power Sources.* **2011**, 196, 7510.
16. V. Puddu, J.M. Slocik, R.R. Naik, C.C. Perry. Titania binding peptides as templates in the biomimetic synthesis of stable titania nanosols: insight into the role of buffers in peptide-mediated mineralization. *Langmuir*. **2013**, 29, 9464-9472.
17. S-J. Park, J.W. Bae,G-I. Jung, K-S. Ha, K-W. Jun, Y-J. Lee, H-G. Park. Crucial factors for catalyst aggregation and deactivation on Co/Al2O3 in a slurry-phase Fischer – Tropsch synthesis. *Appl. Catal. A.* **2012**, 310, 413-414 .
18. E. Roduner. Size matters: why nanomaterials are different. *Chem. Soc. Rev.* **2006**, 35, 583.
19. H-U. Blaser, H. Steiner, M. Studer. Selective catalytic hydrogenation of functionalized nitroarenes: an update. *ChemCatChem*. **2009**, 1, 210

3.0 Formation of 3D Pd Nanostructure by Biomineralization Using an Oligomerized Peptide as the Control Element

3.1. Abstract

The functional dependence of materials to their structure has led to the development of methods with the aim of attaining structural control. One of the most promising methods is biomineralization wherein the peptide aids the formation of mineralized structures. This chapter reports the effects on the formed palladium nanostructures through a designed biomineralization peptide capable of simultaneously supporting palladium growth and forming spatially-fixed oligomers. The designed peptide consists of the Pd-specific sequence (Pd4) and the p53 tetramerization domain (p53Tet). The tetrameric assembly of p53Tet was exploited in order to direct the topology and valency of the Pd4 BMPep. The effect of a topologically assigned BMPep with a fixed valency is evident from the 3D coral-like structures and in the unique tetrahedral orientation of the filaments. These structural observations reflect the critical role assumed by the p53Tet in forming 3D nanostructures.

3.2. Introduction

Hierarchy and organization are hallmarks of natural materials. The outstanding properties of precisely engineered natural materials are attributed to their specialized hierarchical structures [1]. For example, the high mechanical stability of nacre is the direct result of its precisely oriented structure with alternating layers [2]. Hence, an important point in biomimetic approaches of nanomaterial synthesis is the three-dimensional assembly of the biomolecular framework which greatly influences mineralization as well as the properties of the material. [3] As a consequence, precisely controlling the assembly properties of biomineralization peptides have been an important strategy in order to prepare materials with remarkable properties. Here, this chapter describes the design and synthesis of a BMPep that can simultaneously support the growth of palladium as well as precisely assemble into a well-defined three-dimensional framework; wherein the spatial orientation and arrangement are specifically assigned. The strategy involves the fusion of a BMPep to a three-dimensional (3D) control peptide. Porous, hierarchical architecture characterized as coral-like materials were obtained using our designed peptide. The described method overcomes the deficiency of other fusion BMPep hybrids that cannot assign the spatial orientation and arrangement of the BMPep as well as specifying its valency. [4] For example, a portion of the silk protein was recently used to enhance the self-assembly of the attached BMPep. However, the relative arrangement of the BMPep as well as its proportion in the protein assembly was not identified. [5] Organic molecules like biphenyl [6] have also been attached to BMPeps. However, the structures yielded through these methods have been primarily limited to nanoparticles. Hence, fusion BMPep that can exactly direct the topological properties and valency of the BMPep while creating unusual 3D nanostructures is very scarce. In principle, this method can be applied to other metals by simply changing the metal-binding specificity

of the conjugated BMPep. Our method will therefore further widen and broaden the scope of biomineralization as a tool for nanomaterial synthesis.

3.3 Experimental Procedure

3.3.1 Chemicals. All Fmoc-protected amino acids and the rink amide resin used were obtained from Novabiochem whereas the other reagents used in the peptide synthesis such as HOBt, HBTU, piperidine, TFA and solvents were purchased from Watanabe Chem. Ind. Ltd. $NaBH_4$ was purchased from Nacalai-Tesque, K_2PdCl_4 and HEPES were both obtained from Sigma-Aldrich. 2,2'-furildioxime was sourced from Wako Pure Chemical Industries, Ltd. All purchased reagents were used as received without further purification. Milli-Q water was used throughout all experiments.

3.3.2 Peptide Synthesis and Characterization. The peptides (Table 3-1) were synthesized, purified and characterized as described in the previous chapter. The concentrations of the purified Pd4 conjugated variants and the p53Tet were determined by absorption measurements at 280 nm corresponding to the absorptivity of a single tyrosine residue (ε = 1280 $M^{-1}cm^{-1}$) in a denaturing solution composed of 25 mM sodium phosphate (pH 6.5) and 7.5 M Gu•HCl. Due to the absence of a highly absorbing chromophore in the Pd4 peptide, its concentration was determined by mass. Circular dichroism spectra were obtained on a Jasco J-805S spectropolarimeter using a 1 mm quartz cuvette at room temperature. Purified peptides were dissolved at a final concentration of 10 µM in 50 mM phosphate buffer with a pH of 7.4. The secondary structural proportions were calculated using the software SSE-338W. For gel filtration chromatography, a GE Superdex 75 PC 3.2/30 (3.2 mm x 300 mm) column was used. The column temperature was maintained at 25^0C. Separately, 25 µL of 100 µM Pd4-p53Tet and Pd4-p53Mono peptides in 50 mM phosphate buffer with 150 mM NaCl (pH 7.4) were injected. The samples were eluted using the same buffer composition in which the peptides were dissolved with a flow rate of 0.1 mL / minute.

3.3.3 Biomineralization reaction. The peptides were dissolved into a 2.5 mM HEPES-NaOH buffered solution with a pH of 7.4 at a final concentration of 40 μM. Into the solution, a five-fold equivalence of 50 mM K_2PdCl_4 stock solution was added and the resulting peptide – Pd^{2+} solution was incubated for 45 minutes. After this incubation period, an excess of freshly prepared 100 mM $NaBH_4$ was added (800 μM). After the introduction of the $NaBH_4$, the solution color transitioned from yellow to gray. The reduction was allowed to proceed for 90 minutes. Purification of the biomineralization product involved centrifugation at 15000 rpm for 20 minutes wherein the pellet was resuspended in 1 mL of milli-Q water. The homogenous solution was then subjected to electron microscopic analysis.

3.3.4 Electron microscopy. Sample preparation for electron microscopy involved the introduction of 4μL of the purified, re-suspended samples onto a 100 μm copper pitch grid coated with a thin layer of carbon. The prepared copper grids were air and vacuum dried. STEM images, elemental analyses and ion maps were obtained using a Hitachi HD-2000 operating at 200 kV equipped with an EDAX Genesis energy dispersive X-ray. High resolution TEM images and selected area diffraction patterns were obtained using a JEOL JEM-2100F TEM.

Table 3-1. Sequence of synthesized peptides

Peptide	Sequence
Pd4	TSNAVHPTLRHL-amide
Pd4-p53Tet	TSNAVHPTLRHLGGDGEYFTLQIRGRERFEMFRELNEALELKDAQAGKE-amide
Pd4-p53Mono	TSNAVHPTLRHLGGDGEYFTAQARGRERFEMFREANEALELKDAQAGKE-amide
p53Tet	DGEYFTLQIRGRERFEMFRELNEALELKDAQAGKE-amide

3.4 Results

3.4.1 Peptide design and structure analysis

The designed peptide, Pd4-p53Tet is composed of the Pd4 BMPep that was conjugated to the N-termini of the tetramerization domain of the tumor suppressor p53 protein. The Pd4 peptide was discovered through phage display and is specific towards Pd [7]. The p53 tetramerization domain (p53Tet) on the other hand, is one of the five domains of the tumor suppressor p53 protein. The p53Tet is located at the C-terminal region and each monomer within the tetrameric assembly contains a β-strand (residues 326-333), a tight turn (residue 334), and an α-helix (residue 335-356). Two dimers are formed through the formation of a joint antiparallel β-sheet between monomers, and the two primary dimers tetramerize through hydrophobic interactions of the helices in a four-helix bundle. [8] The tetramer was chosen as the 3D control element since the position of its four N-termini is reminiscent of the vertices of the tetrahedron which is the simplest three-dimensional object (Figure 3-1). By utilizing a tetrahedral scaffold, the orientation of the metal binding peptide will have adequate space and the likelihood of each Pd4 BMPep clashing and interacting with each other will be minimized while maintaining a three-dimensional geometry. As a control, the Pd4 BMPep was similarly conjugated to a variant of p53Tet that cannot oligomerize. This monomeric variant of the p53Tet (p53Mono) consists of three alanine substitutions (L330A, I332A and L344A). [9] Other control peptides used include both the native Pd4 and p53Tet sequences.

The CD spectra of the synthesized peptides are shown in Figure 3-2. The Pd4-p53Tet had a similar spectral profile with p53Tet wherein the distribution of their respective secondary structures was predominantly composed of α-helix and β-sheet as what have been expected. This indicates that the Pd4-p53Tet successfully formed tetramers in reference to the

spectrum of the p53Tet. The Pd4 peptide by virtue of its relatively short sequence primarily adopted a random coiled structure. Similarly, the Pd4-p53Mono peptide exhibited a random coiled structure indicating that the alanine substitutions at key residues inhibited the peptide from oligomerizing. The difference between the gel filtration chromatograms of Pd4-p53Tet and Pd4-p53Mono confirms this since smaller peptides have longer retention times over large peptide oligomers (Figure 3-3).

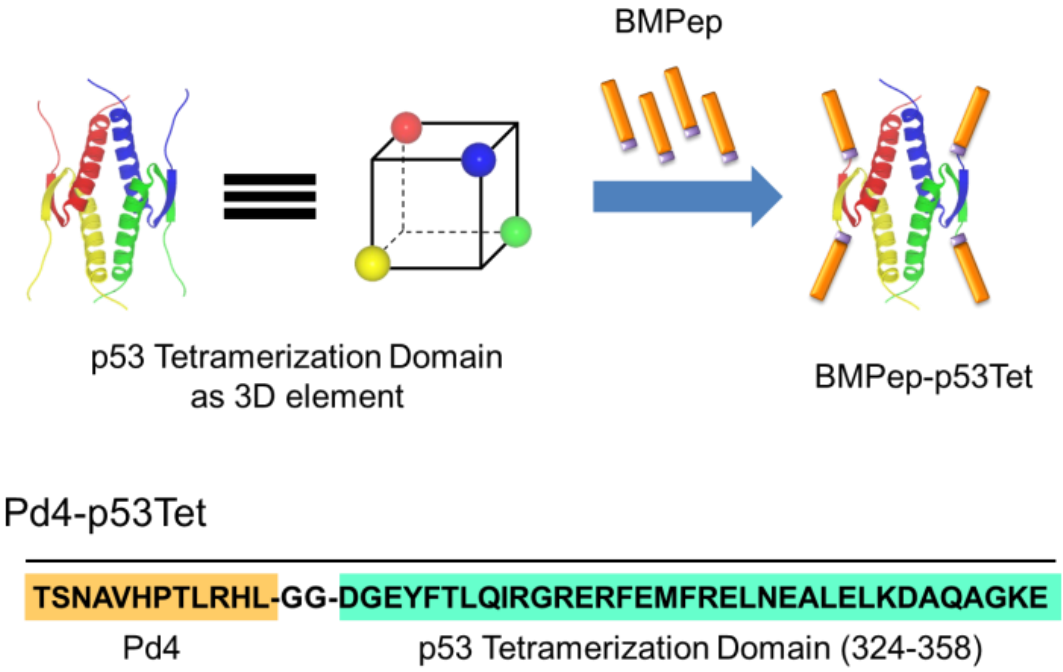

Figure 3-1. Design strategy of a fusion biomineralization peptide with a highly defined three dimensional orientation. The fusion peptide is composed of a BMPep conjugated with a 3D element. The BMPep used is the Pd4 peptide and the 3D element is the p53 tetramerization domain.

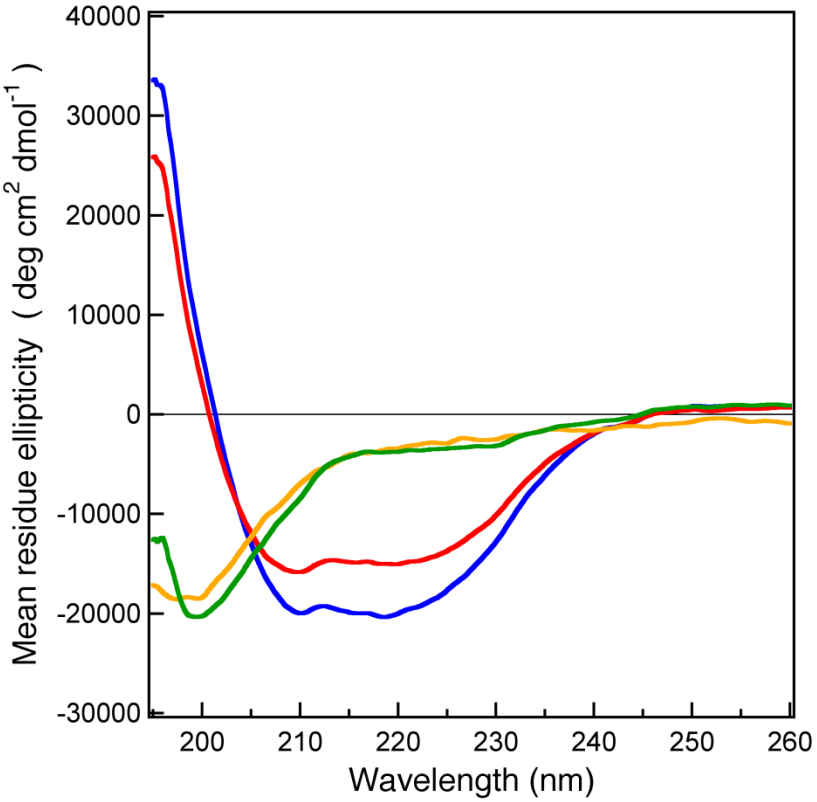

Figure 3-2. Circular dichroism (CD) spectra for the synthesized peptides. Red = Pd4-p53Tet; Blue = p53Tet; Orange = Pd4; Green = Pd4-p53Mono

Table 3-2. Calculated distribution of the secondary structures of the different peptides based on their circular dichroism (CD) spectra

Peptide	α-helix	β-sheet	Turn	Random
Pd4	0	32.1	16.7	51.2
Pd4-p53Tet	36.9	31.7	2.7	28.7
p53Tet	38.8	28.0	6.7	26.5
Pd4-p53Mono	0	34.8	11.8	53.3

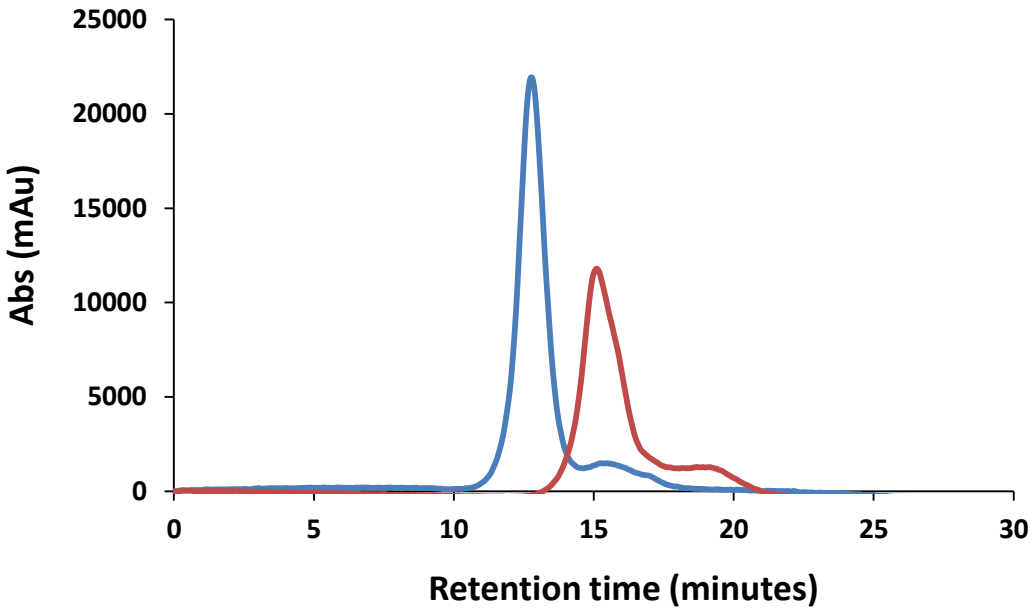

Figure 3-3. Gel filtration chromatogram of Pd4-p53Tet (Blue) and Pd4-p53Mono (Red). The longer retention time of Pd4-p53Mono compared to Pd4-p53Tet confirms that the monomeric variant is incapable of forming tetramers.

3.4.2 Palladium nanostructure synthesis and characterization

The Pd4-p53Tet facilitated the formation of hierarchical and coral-like Pd structures with dimensions such as filament thickness and pore diameters in the nano order. These nanostructures are porous which arises from the network of branched filaments (Figure 3-4A). The absence of lattice lines from TEM images and the halo-like SAED patterns taken at multiple areas indicate that the structures are amorphous (Figure 3-4B). Elemental mapping through EDX (Figure 3-5) confirmed that the structures are made up of Pd. The observed carbon, nitrogen and oxygen signals can be attributed to the incorporation of the peptide with the Pd nanostructures. Moreover, higher resolution analysis using a spot size of 5 nm indicate that both Pd and the peptide are present even at very small areas of the nanocorals (Figure 3-6) It was also often observed that the Pd4-p53Tet derived nanostructures had several filaments at the pore junction oriented in a tetrahedral orientation (Figure 3.4C-D). Comparative structural analysis (Figure 3.7, Table 3-3) was conducted using the native Pd4 sequence, the Pd4-p53Mono, the p53Tet and peptide-free conditions. The negative control yielded aggregated particles. The Pd4 peptide in itself produced uniformly sized and shaped globular aggregates of nanostructured Pd that resembled solid chains. This was in contrast to the irregularly shaped and sized Pd nanoparticles obtained from the p53Tet which were dispersed. Finally, a porous thin film was observed when the Pd4-p53Mono was used as the template. The material produced from the Pd4-p53Mono peptide, which is incapable of assembling into tetramers lack a well-defined and distinct 3D structure.

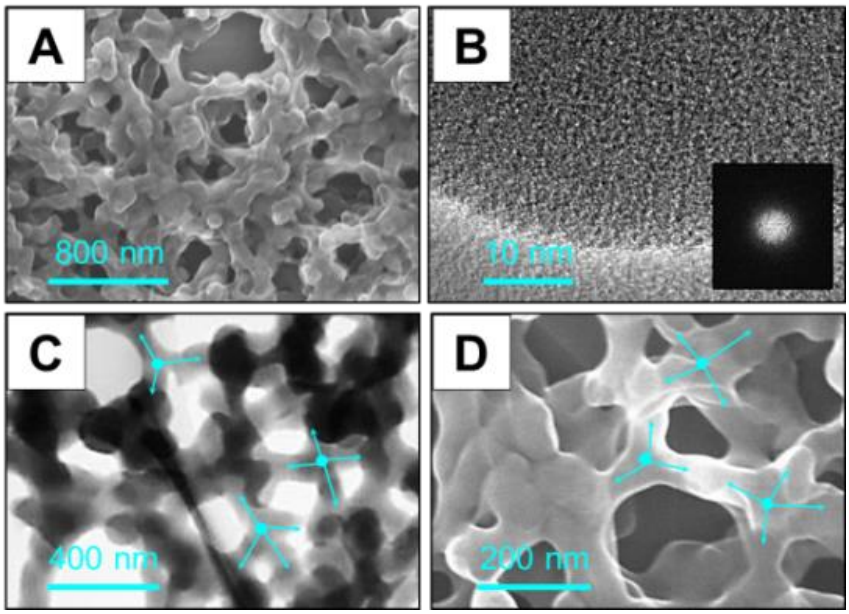

Figure 3-4. Representative electron microscopy images of the coral-like Pd structures derived from the Pd4-p53Tet peptide. **A**) SE-STEM image showing the porous nature of the Pd strucutres which emanates from the branched network of filaments. **B**) HRTEM image focusing on a section of the filament which shows the absence of lattice lines. Inset is the SAED FFT pattern confirming its amorphous nature. **C**-**D**) STEM images showing the tetrahedral orientation of the filaments at different angles.

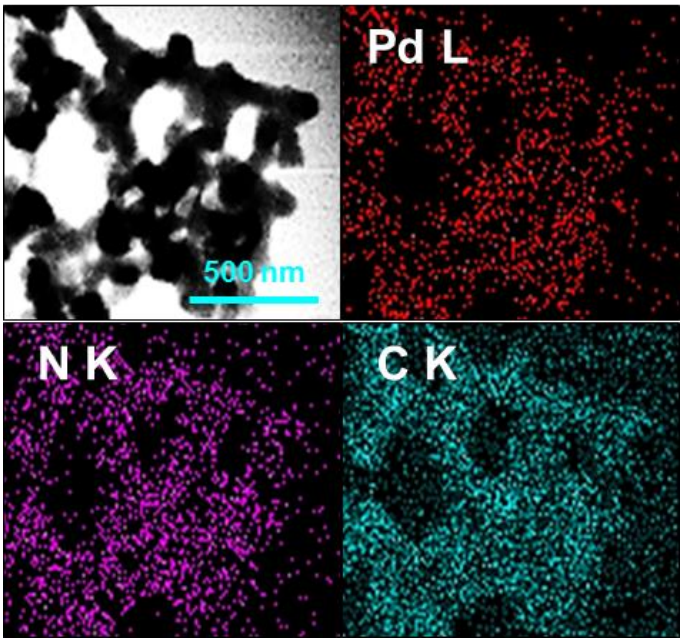

Figure 3-5. EDX elemental mapping of Pd nanocorals from Pd4-p53Tet. From top left clockwise: BF-STEM image of Pd nanocorals, Pd map from L line, N map from K line and C map from K line.

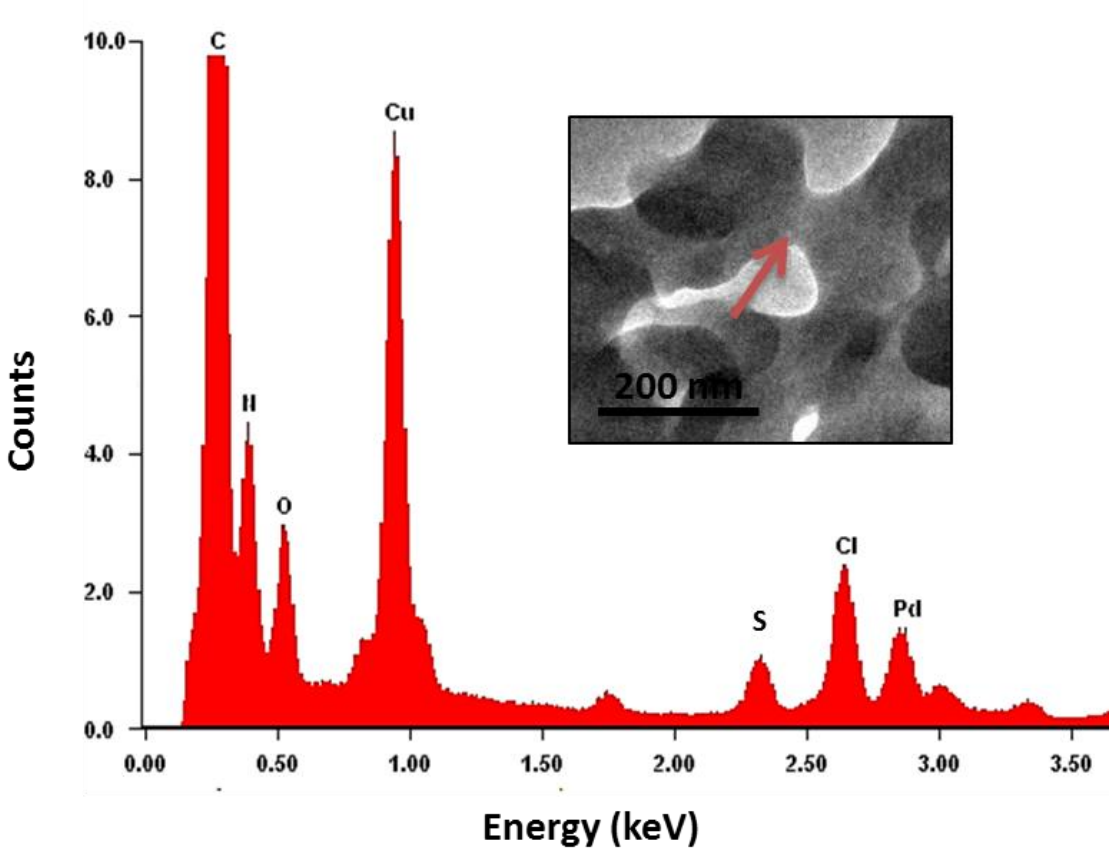

Figure 3-6. EDX spectrum obtained from high-resolution spot measurement using a spot size of 5 nm. Inset picture shows the area of the measurement pointed by the arrow.

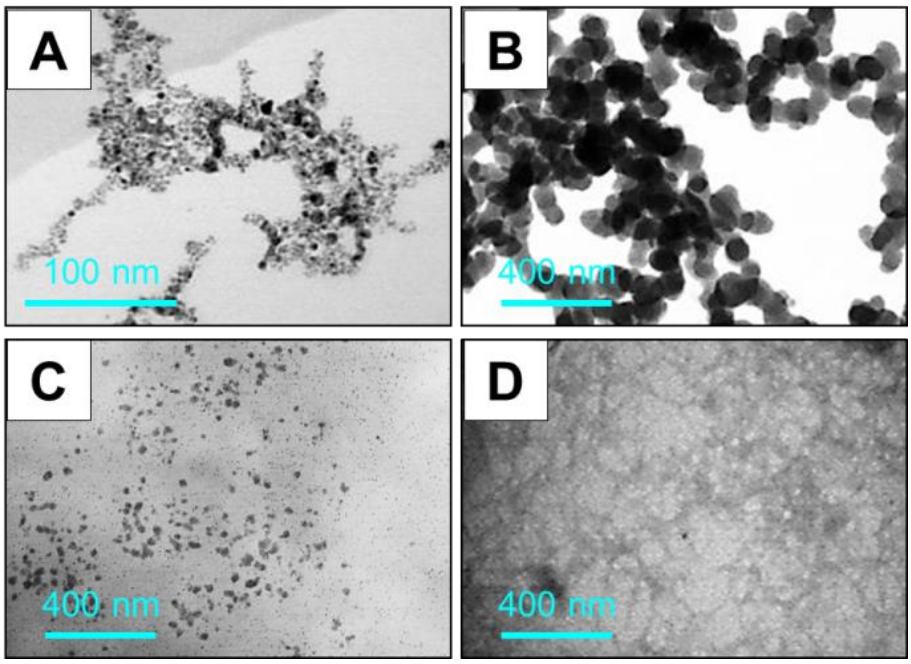

Figure 3-7. BF-STEM images of the Pd nanostructures prepared using peptide sequences **A)** No peptide, **B)** Pd4, **C)** p53Tet, **D)** Pd4-p53Mono.

Table 3-3. Descriptive summary of the Pd nanostructures produced under different conditions

Pd nanostructures	**Size and shape**
Pd4-p53Tet	Porous, coral-like with 3D network (Filament thickness =104 ± 21 nm)
Pd4	Fused, globular particles (Particle diameter =75.3 ± 9 nm)
Pd4-p53Mono	Network of thin filaments (Filament thickness =28.5 ± 10 nm)
No Peptide	Severely aggregated small particles (Particle diameter =2.86 ± 0.62 nm)
p53Tet	Irregularly shaped and sized dispersed particles (Particle diameter =14.4 ± 9 nm)

3.5 Discussion

The presented method shows the simultaneous control over the spatial orientation, arrangement and valency of the BMPep during biomineralization. This assignment of the Pd4 BMPep was achieved through its conjugation with the p53Tet. The faster retention time of Pd4-p53Tet over Pd4-p53Mono in gel filtration chromatography indicates that the designed fusion peptide successfully formed stable tetramers. The designed fusion peptide, Pd4-p53Tet aided the formation of a hierarchical 3D porous material characterized by frequent branching. This porous characteristic is different from the common spherical nanostructure obtained from other biomimetic methods. [10]. Moreover, the nanocorals were also very different from the linearly arranged Pd nanoparticles formed using other BMPep in terms of the structure, size and shape. [11] Furthermore, the 3D branched morphology of the nanocorals was different from the nanostructures obtained from other reported fusion BMPep. To name a few examples, Au nanoparticle double helices were formed when dodecanoic acid was used as the control element in which the Au BMPep was attached. [12] Spherical and rod-like morphologies of Ag were formed when different silk protein sequences were conjugated to Ag BMPep. [13] When a variant of the cowpea virus was used as the control element for Au BMPep, spherical arrangement of Au nanoparticles resembling the shape of the capsid of the virus was observed. [14] The recurring geometric occurrence wherein several filaments were tetra-directional and oriented in a tetrahedral fashion is a consequence of the controlled oligomerization through the p53Tet. The tetrahedral arrangement stems from the spatially-fixed N-termini of the p53Tet from which the Pd4 was conjugated thus validating the rationale for the design of the Pd4-p53Tet. The Pd4-p53Tet peptide effectively acted as a scaffold wherein it was distributed all throughout the coral-like Pd nanostructures. Its presence and wide distribution on the materials explain the amorphous nature of the Pd

structures. The Pd4-p53Tet attaches with the surface of the material rendering the Pd atoms unable to reorganize into ordered crystalline structure. [15]

The comparative analyses reveal that the coral-like appearance, in addition to the tetrahedral spatial arrangement of the filaments, are exclusively observed for the designed Pd4-p53Tet peptide. These results reflect the effect of simultaneously assigning the spatial orientation, arrangement and proportion of the BMPep on the structure of the material. Pd4-p53Tet facilitates nanocoral formation through the combined action of both peptide segments within the Pd4-p53Tet fusion. Moreover, the nanocoral formation follows a multi-step process. Additional experiment revealed that the 45 minute-incubation period of the peptide with Pd ions prior to reduction is necessary to obtain the 3D porous structure. When the incubation period was omitted and reduction was immediately done, flat structures with visibly less porosity were formed (Figure 3-10). This suggests that hierarchical nanostructure formation does not proceed spontaneously and involves multiples steps. The pre-reduction incubation period may be necessary in order for the Pd4-p53Tet to properly assemble. Therefore, it is highly plausible that the Pd nanocoral formation with Pd4-p53Tet proceeds through the following stages (Figure 3-11). The Pd4-p53Tet monomers assemble into a tetramer followed by nanostructure growth at the four Pd4 domains that are spatially-fixed and continues to grow until it is terminated by the linking together of similar units.

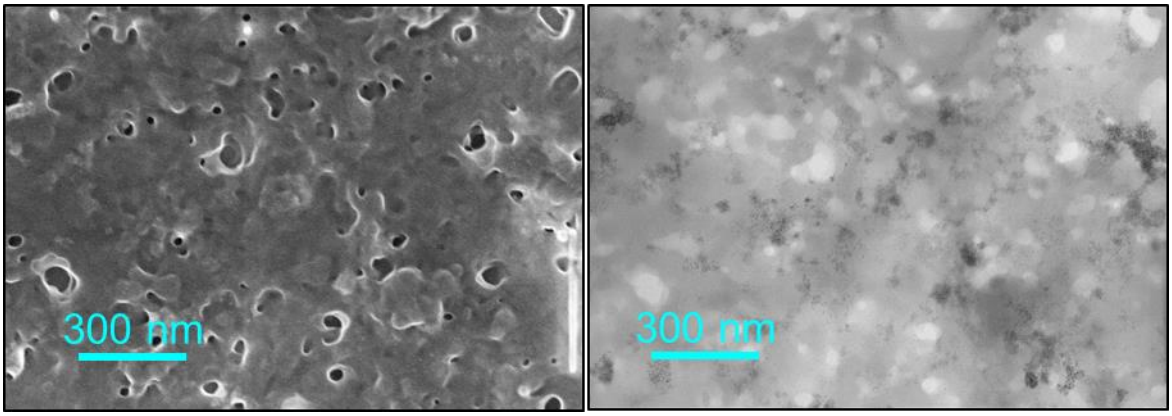

Figure 3-10. SE-STEM (left) and BF-STEM (right) images of Pd nanostructures from Pd4-p53Tet after omitting the pre-reduction incubation period. This control experiment suggests that the formation of the porous, coral-like materials involves a step-wise process

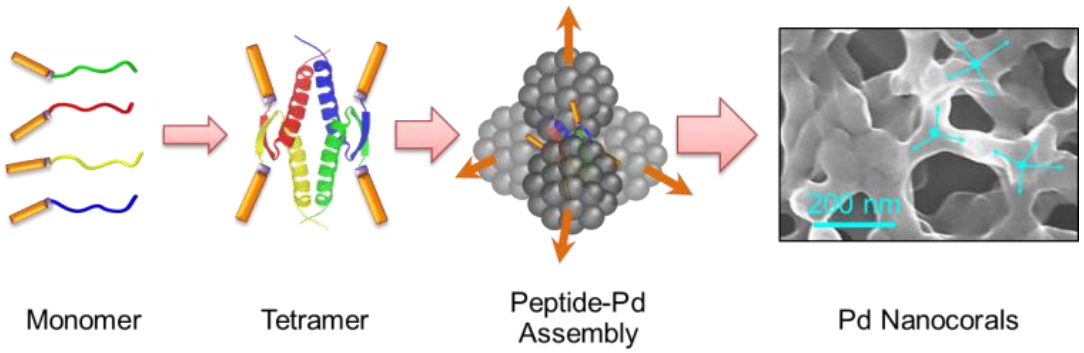

Figure 3-11. Proposed model of Pd nanocoral formation with Pd4-p53Tet. Starting from the monomer of Pd4-p53Tet, the four monomers tetramerize. The spatially-fixed orientation of Pd4 leads to an oriented assembly of growing Pd nanoparticles. Continuous accumulation of Pd at the four sites results to crowding which forces nanostructure growth into tetrahedral directions. Further assembly of similar units yields the hierarchical nanocorals.

3.6. References

1. S. Mann, *Biomineralization: Principles and Concepts in Bioinorganic Materials Chemistry,* Oxford Univ. Press: UK, 2001
2. Y. Oaki, H. Imai. The hierarchical architecture of nacre and its mimetic material. *Angew. Chem. Int. Ed.* 2005, **44**, 6571.
3. F. Nudelman, N. A. J. M. Sommerdijk. Biomineralization as an inspiration for materials chemistry. *Angew. Chem. Int. Ed.* 2012, **51**, 6582-6596.
4. C.L. Chen, N.L. Rosi. Peptide-based methods for the preparation of nanostructured inorganic materials. *Angew. Chem. Int. Ed.* **2010**, 49, 1924-1942.
5. C.W.P.Foo, S.V. Patwardhan, D.J. Belton, B. Kitchel, D. Anastasiades, J. Huang, R.R. Naik, C.C. Perry, D.L. Kaplan. Novel nanocomposites from spider silk-silica fusion (chimeric) proteins. *Proc. Natl. Acad. Sci. U.S.A.* **2006**, 103, 9428-9433.
6. L.Hwang, G. Zhao, P. Zhang, N.L. Rosi. Size-controlled peptide-directed synthesis of hollow spherical gold nanoparticle superstructures. *Small*. **2011**, **7**, 1939-1942.
7. D.B. Pacardo, M. Sethi, S.E. Jones, R.R. Naik, M.R. Knecht. Biomimetic synthesis of Pd nanocatalysts for the Stille coupling reaction. *ACS Nano*. **2009**, 3, 1288-1296.
8. G. M. Clore, J. Ernst. R. Clubb, J.G. Omichinski, W.M.P. Kennedy, K. Sakaguchi, E. Apella, A.M. Groneborn. Refined solution structure of the oligomerization domain of the tumour suppressor p53. *Nat. Struct. Biol.* **1995**, 2, 321-333.
9. R. Kamada, T. Nomura, C.W. Anderson, K. Sakaguchi. Cancer-associated p53 tetramerization domain mutants: Quantitative analysis reveals a low threshold for tumor suppressor inactivation. *J. Biol. Chem.* **2011**, 286, 252-258.
10. R. Bhandari, M.R. Knecht. Isolation of template effects that control the structure and function of nonspherical, biotemplated Pd nanomaterials. *Langmuir*. **2012**, 28, 8110-8119.

11. A. Jakhmola, R. Bhandari, D.B. Pacardo, M.R. Knecht. Peptide template effects for the synthesis and catalytic applications of Pd nanoparticle networks. *J. Mater. Chem.* **2010**, 20, 1522-1531.
12. C.L. Chen, P. Zhang, N.L. Rosi. A new peptide-based method for the design and synthesis of nanoparticle superstructures: construction of highly ordered gold nanoparticle double helices. *J. Am. Chem. Soc.* **2008** 130, 13555-13557.
13. H.A. Currie, O. Deschaume, R.R. Naik, C.C. Perry, D.L. Kaplan. Genetically engineered chimeric silk-silver binding proteins. *Adv. Funct. Mater.* **2011**, 21, 2889-2895.
14. J.M. Slocik, R.R. Naik, M.O. Stone, D.W. Wright. Viral templates for gold nanoparticle synthesis. *J. Mater. Chem.* **2005**, 15, 749-753.
15. C.H. Lu, F.C. Chang, F. Polyhedral oligomeric silsesquioxane-encapsulating amorphous palladium nanoclusters as catalysts for Heck reactions.*ACS Catal.* **2011**, 1, 481-488.

4.0 Effects of the Biomineralization Peptide Topology on the Catalytic Activity of Pd Nanomaterials

4.1. Abstract

The effects of the biomineralization peptide topology and valency on the catalytic activity of Pd nanomaterials are herein examined. The Pd nanocorals obtained by using the previously designed fusion peptide (Pd4-p53Tet) whose topological arrangement and valency are assigned were used as catalysts for the reduction of nitrophenol. The Pd nanocorals exhibited excellent catalytic activity towards this reaction which suggests that designing materials with highly-defined 3D character could potentially lead to high-performance materials. The 3D properties of the material depend on the 3D properties of the biomineralization peptide. Therefore, assigning the biomineralization peptide topology and valency is a viable approach towards the formation of efficient catalysts.

4.2. Introduction

The advantages achieved in using biomineralization as a synthetic route towards inorganic nanomaterial synthesis have initiated efforts to understand this matter deeper. Recently, attempts to elucidate the different factors that govern biomineralization have been carried out. From these reports, it has been shown that the BMPep structure, [1] BMPep sequence, [2] nature of BMPep binding onto the material surface, [3] BMPep-metal equivalence, [4] buffer type [5] and amount of reductant [6] can affect the structure and catalytic activity of nanomaterials formed from biomineralization. It has also been reported that the structure of the BMPep acting as a scaffold can also affect the nanostructure and catalytic activity of the biomineralization products. [7] Therefore, if the spatial orientation, arrangement and valency of the BMPep can be simultaneously defined, this may have a tremendous impact not only on the resulting nanostructure but also with the catalytic performance of the materials. In the previous chapter, a fusion biomineralization peptide whose valency and topological arrangement are well-defined have been presented. Through this designed fusion peptide, coral-like, branched and 3D porous Pd nanostructure were formed. In this chapter, the catalytic activity of the Pd nanocorals is evaluated. This is done in order to examine the effects of defining the topological properties and valency of the BMPep on the catalytic activity of Pd nanomaterials.

4.3. Experimental Procedure

4.3.1. Chemicals. 4-nitrophenol was purchased from Nacalai-Tesque; 2,2'-furildioxime was sourced from Wako Pure Chemical Industries, Ltd.; 2-nitrophenol and 3-nitrophenol were obtained from Tokyo Chemical Industry, Co. Ltd. All purchased reagents were used as received without further purification. Milli-Q water was used throughout all experiments.

4.3.2. Biomineralization reaction. The Pd nanomaterials which will serve as catalysts were prepared in a similar manner as what have been descried in the previous chapter.

4.3.3. Catalytic reaction. The palladium content of the Pd4-p53Tet-based materials and the nanoparticles obtained from peptide free conditions was determined spectrophotometrically with the aid of 2,2'-furildioxime as the complexing ligand [8]**.** In a typical procedure, 0.1 mL of purified material was dissolved in concentrated HCl. The resulting solution was evaporated after which the Pd ions were complexed with 5 mM of the ligand in an acidic environment. The resulting complex was bright yellow and its absorbance was immediately measured at 425 nm. From a standard curve, the palladium content of the materials was determined.

For the reduction of the nitrophenol isomers, 10 µL of 5 mM nitrophenol was added to an excess of $NaBH_4$ to give a final concentration of 100 mM (200 fold excess). Subsequently, the necessary amount of the purified Pd material to give a final concentration of 0.42 µM Pd (0.8 mol %) was added to the solution. The progress of the reaction was monitored by UV-vis for 5 minutes with measurements taken every second (4-nitrophenol λ_{max} = 398 nm; 3-nitrophenol λ_{max} = 391 nm; 2-nitrophenol λ_{max} = = 414 nm) . From the absorbance readings, the pseudo-first order rate constants were calculated

as well as the turnover frequency for each reaction. All quantitative analyses were conducted in triplicate.

4.4. Results

4.4.1. Catalytic activity of Pd4-p53Tet Pd nanocorals

The catalytic performance of Pd4-p53Tet Pd nanocorals was assessed using the reduction of nitrophenol to aminophenol as the model reaction (Scheme 4-1). This reaction is ideal to probe the catalytic properties of materials since the reactants must be adsorbed onto the material surface in order for the reaction to proceed. In addition, this reaction can be easily monitored by the progression of color loss. In this reaction, $NaBH_4$ serves as the reducing agent in order for the reduction to proceed. All the nitro substrates yielded colored solutions in the presence of $NaBH_4$, whereas their corresponding amino products are colorless. In the absence of a metal catalyst, the reduction of the nitro moiety does not occur. In contrast, the color of the solution diminishes immediately upon the introduction of a metal catalyst. The large excess amount of $NaBH_4$ used justifies the pseudo-first order assumption since the change in its concentration is negligible. Thus, the integrated rate law ($\ln C_t = -kt + \ln C_0$) for a first order reaction was applied in order to determine the rate constant for the reduction. The rate constant corresponds to the slope of the graph in which $\ln C_t$ was plotted as a function of time. The nanocorals exhibited high catalytic efficiency on the basis of the higher turnover frequency (TOF) for the three different substrates compared from other reports in literature. [9-11] The Pd4-p53Tet nanocorals possessed much higher activity than the materials from Pd4, Pd4-p53Mono and no peptide materials with respect to the TOF and rate constants (Figure 4-2, Figure 4-3, Table 4-1). On the other hand, the materials derived from p53Tet had similarly competitive catalytic activity with the Pd4-p53Tet nanocorals.

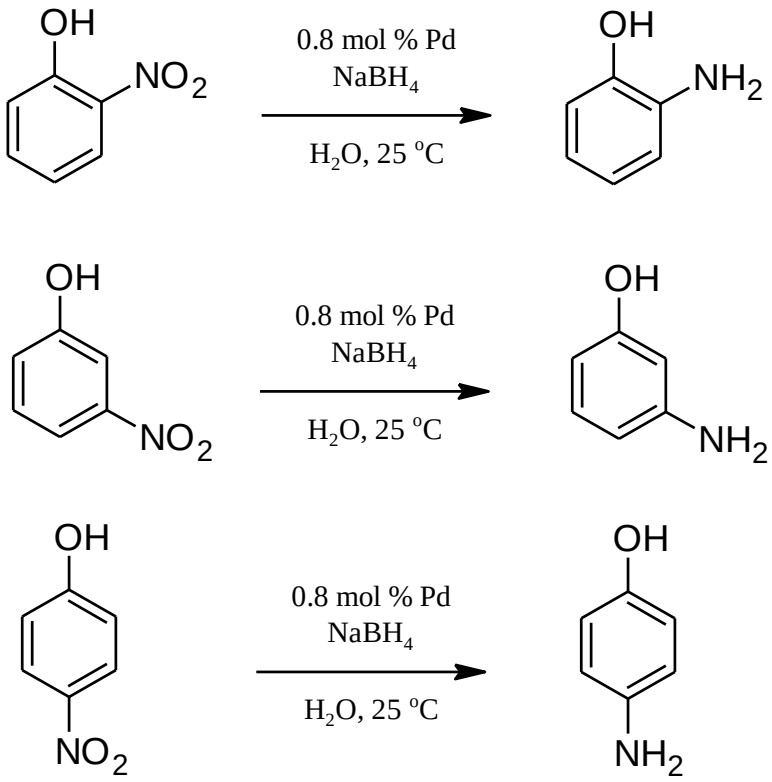

Scheme 4-1. Reduction of the nitrophenol isomers into the corresponding aminophenol products.

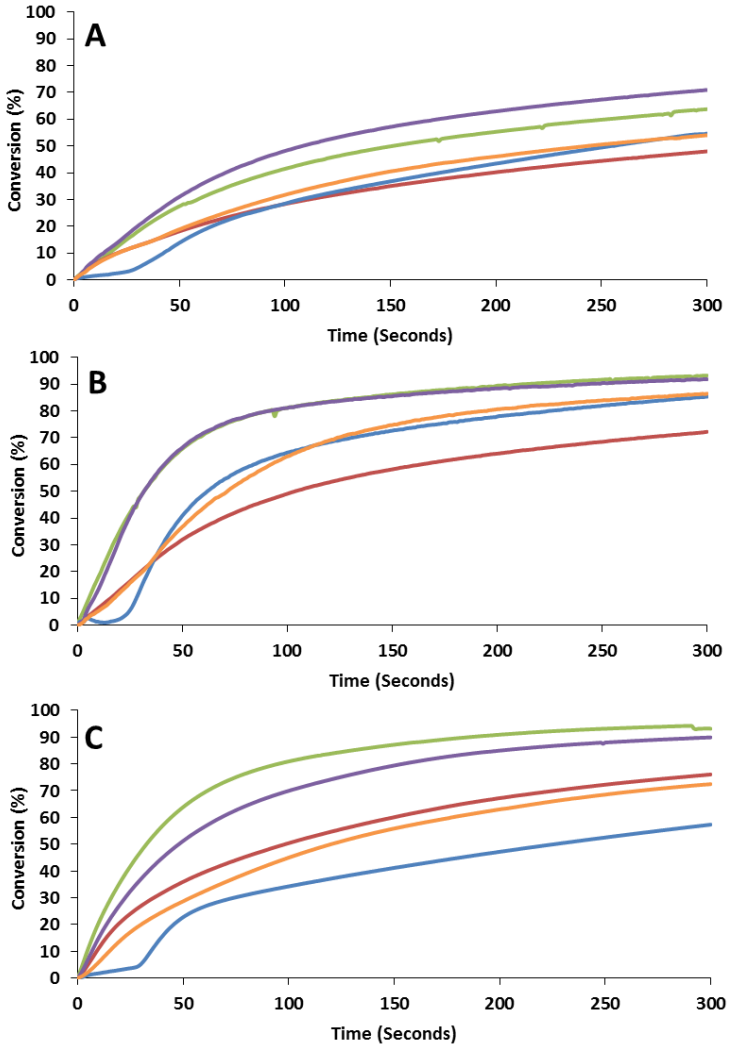

Figure 4-1. Time course reduction of nitrophenol isomers (Triplicate analyses, continuous measurement, 1 second interval). **A)** 2 – nitrophenol, **B)** 3- nitrophenol, **C)** 4-nitrophenol. Green = Pd4-p53Tet Pd nanocorals, Red = No Peptide Pd nanoparticles, Blue = Pd4 Pd nanoparticles, Purple = p53Tet Pd nanostructures, Orange = Pd4-p53Mono Pd nanostructures

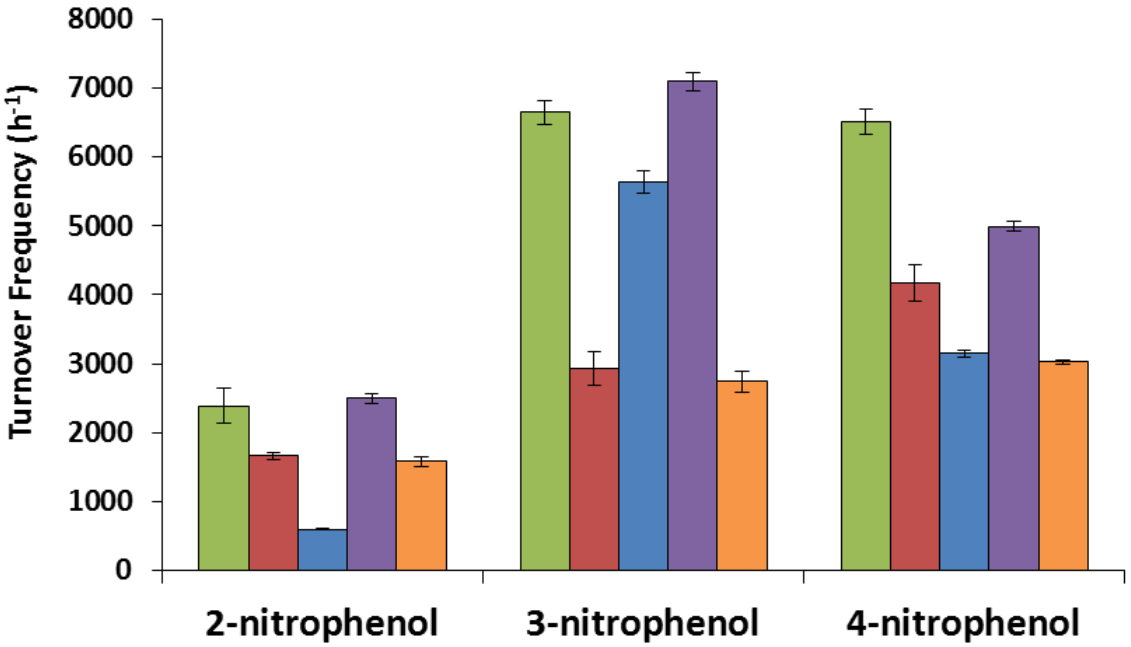

Figure 4.2. Turnover frequency (TOF) comparison among the different Pd nanomaterials prepared by biomineralization under different conditions. Green = Pd4-p53Tet Pd nanocorals, Red = No Peptide Pd nanoparticles, Blue = Pd4 Pd nanoparticles, Purple = p53Tet Pd nanostructures, Orange = Pd4-p53Mono Pd nanostructures

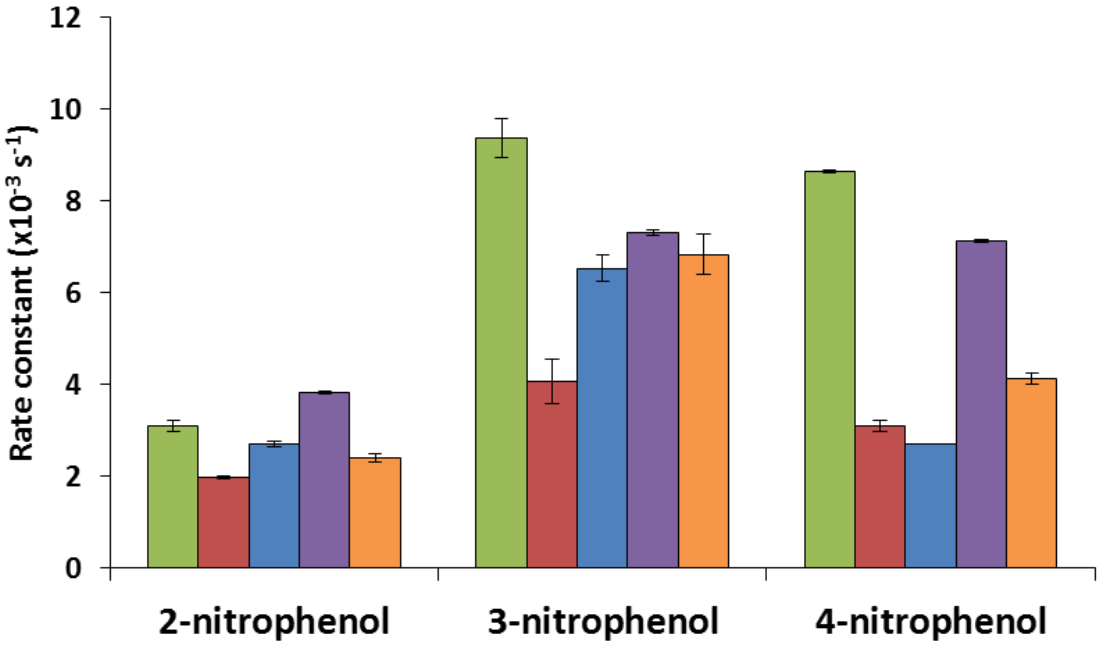

Figure 4.3. Pseudo-first order rate constant comparison among the different Pd nanomaterials prepared by biomineralization under different conditions. Green = Pd4-p53Tet Pd nanocorals, Red = No Peptide Pd nanoparticles, Blue = Pd4 Pd nanoparticles, Purple = p53Tet Pd nanostructures, Orange = Pd4-p53Mono Pd nanostructures

Table 4-1. Shape, size and catalytic data of the Pd nanomaterials formed from different BMPep for the reduction of nitrophenol isomers.

	Shape and size	Turnover Frequency (h^{-1}) (Pseudo-first order rate constants (k, $x10^{-3}$ s^{-1}))		
		2-nitrophenol	3-nitrophenol	4-nitrophenol
Pd4-p53Tet	Porous, coral-like with 3D network (Filament thickness =104 ± 21 nm)	2390 ± 440 (3.10 ± 0.20)	6650 ± 300 (9.37 ± 0.74)	6510 ± 300 (8.63 ± 0.06)
Pd4	Fused, globular particles (Particle diameter =75.3 ± 9 nm)	600 ± 10 (2.70 ± 0.10)	5640 ± 290 (6.53 ± 0.50)	3150 ± 90 (2.7 ± 0)
Pd4-p53Mono	Network of thin filaments (Filament thickness =28.5 ± 10 nm)	1580 ± 120 (2.4 ± 0.10)	2740 ± 270 (6.83 ± 0.45)	3020 ± 60 (4.13 ± 0.12)
No Peptide	Severely aggregated small particles (Particle diameter =2.86 ± 0.62 nm)	1660 ± 100 (1.97 ± 0.06)	2930 ± 410 (4.07 ± 0.85)	4170 ± 460 (4.23 ± 0.21)
p53Tet	Irregularly shaped and sized dispersed particles (Particle diameter =14.4 ± 9 nm)	2500 ± 120 (3.83 ± 0.06)	7100 ± 240 (7.30 ± 0.10)	4990 ± 130 (7.13 ± 0.06)

Average size was determined from a minimum of 100 measurements. Numbers in parenthesis correspond to the pseudo-first order rate constants. Numbers above the rate constants are the TOF. Conditions: [Substrate] =50 μM, [Pd] =0.8 mol%, [$NaBH_4$] =10 mM, 25^0C, triplicate analyses.

4.5. Discussion

The excellent catalytic performance of the Pd nanocorals, characterized by competitive TOF and rate constant values can be attributed to the unique 3D branched structure. The structure of the Pd nanocorals is defined by a high degree of filament cross-links in different directions. The turnover frequency is an important descriptor of catalyst efficiency. It is defined as the number of reaction cycles the catalyst can facilitate before deactivation happens at a given period of time. [12] On the other hand, the rate constant provides an idea to how fast the reaction proceeds in the presence of a catalyst. Thus, it can be seen that the Pd nanocorals are efficient and active catalysts. The 3D structure of the materials can influence catalyst reactivity. [4] On the other hand, the structures from Pd4 and Pd4-p53Mono share the linked morphological feature with the nanocorals but obviously had less 3D character. Comparing the activities of the materials from Pd4-bearing sequence suggests that increasing the 3D character of the material can lead to the formation of catalysts that are capable to greatly accelerate the reaction as well as facilitate reactant turnover. The nanoparticles from peptide-free conditions showed low activity, both in terms of TOF and rate constants. This is most likely due to the aggregation of the particles. In contrast were the p53Tet-derived materials which had high catalytic activity. The high activity can be attributed to the small and dispersed nature of the particles which commonly result to favorable catalytic properties such as alteration of the electronic properties, high surface area, among others. [13] Comparing the activities of Pd4-p53Tet and p53Tet raises an interesting observation. The nanocorals were very active despite their larger size. This strongly suggests that the materials with a highly defined 3D structure could give rise to the formation of excellent catalysts. Assigning the topological properties of the BMPep therefore affects not only the nanostructure but the catalytic properties as well. This highlights the importance of specifying the 3D property of the template since the 3D structure of the material depends on

it, which influences the catalytic activity. This information expands the knowledge on other known factors that can influence the nanostructure and the catalytic properties of nanocatalysts formed from biomineralization such as the BMPep sequence, [2] nature of the BMPep adsorbed on to the nanomaterial surface, [3] metal salt equivalence, [4] and presence of a buffer [5] among others.

4.6. References

1. N. Choi, L. Tan, J. Jang, Y.M. Um, P.J. Yoo, W-S. Choe. The interplay of peptide sequence and local structure in TiO2 biomineralization. *J. Inorg. Biochem.* **2012**, 115, 20-27.
2. R. Coppage, J. M. Slocik, M. Sethi, D.B. Pacardo, R.R Naik, M.R. Knecht. Elucidation of peptide effects that control the activity of nanoparticles. *Angew. Chem. Int. Ed.* **2010**, 49, 3767-3770.
3. Y. Li, Z. Tang, P.N. Prasad, M.R. Knecht, M.T. Swihart. Peptide-mediated synthesis of gold nanoparticles: effects of peptide sequence and nature of binding on physicochemical properties. *Nanoscale*. 2014, **6**, 3165-3172.
4. R. Bhandari, M.R. Knecht. Effects of material structure on the catalytic activity of peptide-templated Pd nanomaterials. *ACS Catal.* 2011, **1**, 89-98.
5. J.I.B. Janairo, K. Sakaguchi. Effects of the buffer on the structure and catalytic activity of Pd nanomaterials formed by biomineralization. *Chem. Lett.* **2014**, DOI: 10.1246/cl.140405
6. C.Y. Chiu, Y. Li, Y. Huang. Size-controlled synthesis of Pd nanocrystals using a specific multifunctional peptide. *Nanoscale*. **2010**, 2, 927-930.
7. R. Bhandari, M.R. Knecht. Isolation of template effects that control the structure and function of nonspherical, biotemplated Pd nanomaterials. *Langmuir*. **2012**, 28, 8110-8119.
8. O. Menis, T.C. Rains. Colorimetric determination of palladium with alpha-furil dioxime. *Anal. Chem.* **1955**, 27, 1932-1934.
9. J**.** Li, X.Y. Shi, Y.Y. Bi, J.F. Wei, Z.G. Chen. Pd nanoparticles in ionic liquid brush: a highly active and reusable heterogeneous catalytic assembly for solvent-free or on-water hydrogenation of nitroarene under mild conditions. *ACS Catal*. **2011**, 1, 657-664.

10. Q. Wang, W. Jia, B. Liu, A. Dong, X. Gong, C. Li, P. Jing, Y. Li, G. Xu, J. Zhang. Hierarchical structure based on Pd(Au) nanoparticles grafted onto magnetite cores and double layered shells: enhanced activity for catalytic applications. *J. Mater. Chem. A.* **2013**, 1, 12732-12741.
11. X. Wu, C. Lu, W. Zhang, G. Yuan, R. Xiong, X. Zhang. A novel reagentless approach for synthesizing cellulose nanocrystal-supported palladium nanoparticles with enhanced catalytic performance. *J. Mater. Chem. A.* **2013**, 1,8645-8652.
12. *Catalysis, Concepts and Green Applications*, by G. Rothenberg, Wiley-VCH, Germany, **2008**
13. J.D. Aiken III, R.G. Finke. A review of modern transition metal nanoclusters: their synthesis, characterization, and application in catalysis. *J. Mol. Catal. A: Chem*, **1999**, 145, 1-44.

5.0 Conclusion

In conclusion, the work presented systematically analyzed the effects of two different parameters on the structure and catalytic activity of Pd nanomaterials formed from biomineralization. This study has successfully achieved precise control over the spatial orientation, arrangement and valency of the BMPep. This was done through an elegant technique of using a self-oligomerizing peptide as the 3D control element from which the BMPep was conjugated to. As a proof of concept, the p53Tet was used as the 3D control element which resulted to a tetrahedral orientation of the Pd4 BMPep within the tetrameric assembly. By using this designed fusion peptide, highly branched, porous and coral-like Pd nanostructures were produced which exhibited high catalytic activity. The high catalytic activity of the Pd nanocorals, despite having a large size can be attributed to the well-defined 3D character. Having the ability to control the spatial and order of the BMPep at this level of precision represents an important advancement given that hierarchy and order and the hallmarks of nature-made materials. In addition, the study has expanded the knowledge regarding the factors that affect the nanostructure and catalytic activity of materials formed from biomineralization, such as the BMPep sequence and metal stoichiometry. The developed method also exhibits both generality and versatility since other BMPep may be similarly conjugated with the p53Tet thus providing a very flexible method for biomineralization control that can be fine-tuned by choosing a specific BMPep.

This study has further shown that maintaining the pH and the presence of a buffer have significant effects on the structure and morphology of the Pd biomineralization products. In turn these structural variations influence the catalytic activity of the materials. Therefore, buffer selection is critical for Pd biomineralization and should be considered carefully. Through this, a facile and cost-effective method of enhancing the catalytic activity of Pd nanomaterials formed from biomineralization has been brought forward. Conducting

biomineralization in buffered medium is far easier and simpler compared with other means of enhancing the performance of Pd nanomaterials.

By and large, the study has expanded the knowledge regarding the factors that affect the nanostructure and catalytic activity of materials formed from biomineralization. Moreover, this study has aided in the deeper understanding of biomineralization by providing new and concrete insights regarding the influence of these new tunable parameters, namely the biomineralization peptide topology and valency, as well as the buffer. This study has brought forward the idea that biomineralization can be enhanced in terms of the structure and catalytic activity of the resulting nanomaterials by regulating the BMPep 3D structure and through careful buffer selection.

It is a promising endeavor to extend the findings of this work to bimetallic materials. This class of materials is involved in a wide variety of applications due to the synergism that exists between the two metal components. Using a biomineralization peptide whose 3D structure and valency are well-defined may lead to the formation of bimetallic materials with remarkable properties.

6.0 Acknowledgement

"Laborare est orare ~ to work is to pray"

With the completion of this thesis, I duly recognize the constant presence of God which has made all of these possible.

I would like to sincerely thank the Japanese Government, through MEXT for this generous opportunity to conduct my Ph.D studies at Hokkaido University as a Monbukagakusho scholar. I dedicate this thesis to my family, especially to my parents, Dr. Gerardo Janairo and Susana Janairo for their relentless support and encouragement. To my older sister, Isabel and her husband Alvin, to my younger sister, Ilona, to my adorable niece, Ianna, and to my girlfriend, Linley.

I am very grateful for the guidance, understanding and support of my supervisor and mentor, Prof. Kazuyasu Sakaguchi. I have learned so many things from Sakaguchi-sensei, not only about science but also on being a scientist. I am also very thankful for the support from the staff and fellow students of our laboratory. To Dr. Toshiaki Imagawa, Dr. Yoshiro Chuman and Dr. Rui Kamada. I would like to especially mention my student supporter, Yuuki Kozakai for all of her assistance which helped me adjust to my new environment. The assistance extended by Fukuoka-sensei and especially to Hara-sensei is highly appreciated and valued.

I am thankful for the helpful comments and encouragements from my thesis committee composed by Prof. Yota Murakami, Prof. Koichiro Ishimori, Prof. Seiichi Taguchi and Dr. Toshiaki Imagawa.

I would like to thank my master course adviser, Dr. Derrick Yu, not only for helping me during the scholarship application but also for his constant concern, guidance and

encouragement. I am thankful for the continuous support and concern of my undergraduate thesis adviser, Dr. Nancy Lazaro-Llanos, all throughout my studies Finally, I would like to thank my friends both here in Japan and at home. To Ate Lelyn, Ate Fej, Ate Mae, Roger, Fatsy, Lea, members of the English Mass Community, Hokkaido Association of Filipino Students (HAFS), Samahang Pilipino sa Hokkaido (SPH), Eric and Maryanne. *Maraming salamat!*